Proposal for an Integrated Raman-free Correlated Photon Source

By

Daniel Blay

A thesis submitted to Macquarie University
for the degree of Master of Research
Department of Physics and Astronomy
December 2015

Acknowledgements

I would like to thank my parents, and my family as a whole, for their support throughout the year and my life. Even when they didn't understand what I was doing, or why. I promise it all means something.

I would especially like to thank my supervisors, Mike Steel and Luke Helt, for their infinite patience and understanding. Not to mention tolerance of my humour. None of this would have been possible if not for their efforts.

I must not forget the administrative staff, who keep the department running like a well-oiled toaster oven. Their job isn't easy – managing physicists is like herding absent-minded cats.

For my friends, who have made it very clear that help is always available, and good times and food never far away. Thank you to my fellow students, who certainly have kept me from getting a big head, and for their abundance of good (and bad!) advice.

Lastly thank you to one of my closest friends and confidants throughout my life, my dog Rusty, who is no longer with us.

Abstract

The on-demand generation of identical single photons is one of the most keenly sought capabilities in quantum optics. Such sources are a key resource in optical implementations of quantum information processing, such as quantum communication or computing.

Many current heralded single-photon sources use the third order nonlinear optical process of spontaneous four wave mixing, whereby two pump photons are converted into a signal photon and an idler photon. These sources can be based on integrated or fibre platforms, but suffer from the spontaneous generation of Raman-shifted photons, particularly in amorphous materials. This noise limits their utility, as heralding detectors cannot distinguish between genuine pairs produced by the source and unpaired single photons.

In this thesis, we propose and theoretically analyse a new photon generation method we term "Stimulated Spontaneous Three Photon Down Conversion". Pumping a nonlinear material at the third harmonic, we spontaneously generate three photons at the fundamental frequency – spectrally isolated from the Raman noise around the pump. A weak seed beam near the fundamental frequency leads to an increase in the rate of correlated pairs produced on either side of the seed, resulting in an effective heralded single-photon source of much-reduced noise. We work in the framework of a fully multi-mode Hamiltonian formalism of nonlinear quantum optics. Applying this technique in fused silica microfibre could in principle produce 0.03 pairs per pulse, with realistic pump field requirements.

Contents

Anything worth taking seriously
is worth making fun of.

Tom Lehrer

1 Introduction

Since the taming of fire, humanity has had the ability to produce vast quantities of *photons* – discrete packets of light. The humble 40 W incandescent light bulb produces hundreds of quintillions ($\sim 10^{20}$) of optical photons per second. Producing only *single* photons on demand, however, is another matter entirely. This capability is sought after worldwide in the quantum optics and information community, as it would allow for a deeper probing of the quantum world, as well as the development of incredible new technologies. This includes quantum computers [1], which if realised will be able to solve problems that current "classical" computers find intractable. Another example is quantum communication, which in principle allows for the 100% secure transmission of a key for the encryption and decryption of messages through a technique known as Quantum Key Distribution (QKD) [2].

Photons, through the lens of quantum optics, are well-suited to the task of unlocking the potential of the quantum world. Unlike matter-based quantum objects, they have long coherence times. They are relatively easy to generate in entangled states (for example, passing an indistinguishable pair of photons through a beam splitter generates a *NOON state* with $N = 2$, represented as $|\psi\rangle = \frac{1}{\sqrt{2}}(|N, 0\rangle + |0, N\rangle)$ [3]). They are easy to transport as they propagate naturally. In particular, photons produced in the 1550 nm band can be transported long distances over optical fibre with minimal disruption. Although subject to scattering and absorptions, photons do not decay. However, there is more to a photon than just $\hbar\omega$.

1.1 What is a photon?

A photon is the discrete excitation of the electromagnetic field, possessing a distribution of frequencies, spatial structure, a polarisation and a momentum. It is common in the field of quantum information to see the single photon represented as $|1\rangle = \hat{a}^\dagger |0\rangle$ where $\hat{a}^\dagger$ is the usual creation operator associated with the quantum harmonic oscillator, and $|n\rangle$ represents a state containing n photons, with $|0\rangle$ being the vacuum state. However, this does not capture any of the aforementioned degrees of freedom, such as which mode the operator $\hat{a}^\dagger$ corresponds to[1]. If we wish to capture several degrees of freedom, we can represent this state more realistically as

$$|\psi\rangle = \sum_{i,\sigma} \int \mathrm{d}\omega \, f_{i,\sigma}(\omega) \hat{a}^\dagger_{i,\sigma,\omega} |0\rangle, \tag{1.1}$$

where f describes the frequency distribution and $\hat{a}^\dagger$ is now indexed by the mode i, polarisation σ and the frequency ω. The quantum nature of this object lies in the non-trivial algebra satisfied by $\hat{a}$ and the ability to produce superpositions of states.

This thesis considers a new method of single photon generation, based on nonlinear optical processes. The need for a new source is motivated by the pressing issue of *spontaneous Raman scattering* in amorphous materials, which many current *spontaneous four wave mixing* (SFWM) sources rely on. We will gain more insight into this problem in section 1.2.

1.2 How do we make photons?

An ideal *photon source* would be one for which we could control every degree of freedom simultaneously and generate single photons on demand. We can imagine a device like the one shown in fig. 1.1, which produces a single photon with the desired characteristics upon every press of the button, or at least on most presses (we cannot beat the second law of thermodynamics). Unfortunately the engineering demands on such a contraption are, for now, too great, but we can try to constrain as many as possible when designing real sources.

Photon sources must address several challenges. For most quantum applications, we require a high rate of photons since many protocols require multiple photons and the efficiency of these protocols grows with higher power. They must produce truly 'single' photons ($\langle\psi| \hat{N} |\psi\rangle = \sum_{i,\sigma} \int \mathrm{d}\omega \, |f_{i,\sigma}(\omega)|^2 = 1$, where $\hat{N}$ is the number operator). The source must be tailored to have the desired correlations between photons, or lack-thereof (be it frequency, spatial or temporal correlation), and desired spectral properties. Such sources must produce photons which are "indistinguishable" from each other (in all but one degree of freedom).

[1]Here *mode* refers to the spatial eigenfunctions of the modal wave equation. Examples include the familiar HE and LP modes of an optical fibre.

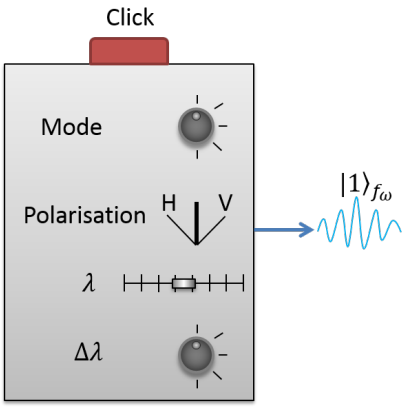

Figure 1.1: A device for which we control all of our degrees of freedom, press the button, and produce precisely the photon we want.

Furthermore, many applications, such as quantum computing, require that the source is scalable, as we must be able to produce them en masse.

There are two main schemes in use today for producing single photons that satisfy most of these requirements: single quantum or atom-like systems and nonlinear optical schemes. The former typically involve placing single photon emitters like atoms into cavities, where they couple with the cavity field. Such emitters include "two level" atoms [4], quantum dots [5], nitrogen vacancies in diamond crystals [6] and colour centres in other crystal lattices [7].

Many atom-like emitters require complex laser systems, for example to generate optical lattices for atom trapping [8], and must be placed in ultra-high vacuum chambers to maintain isolation from their environment. Even then, the lifetime of such systems can be short and as a result, they are often bulky and unsuitable for many applications. Some of these requirements have been relaxed by the fabrication of solid-state microcavities, which are highly compact [9]. However, most systems still must be cooled to cryogenic temperatures (often done with liquid helium), requiring further equipment. Notable exceptions include nitrogen and silicon vacancy centres in diamond, which can operate at room temperature [10, 11]. However due to difficulties in fabrication, reliably producing indistinguishable photons (due to inconsistent quantum dot fabrication, as an example) can be problematic. Despite these shortcomings atom-like systems can produce high quality single photons, and are likely to ultimately become the preferred source.

In contrast with atom-like systems, Nonlinear Optics (NLO) takes advantage of higher order electric susceptibilities (typically the second and third order susceptibilities, denoted by $\chi^{(2)}$ and $\chi^{(3)}$ respectively) in various materials to convert light at one or more frequencies into other frequencies. Owing to the very weak nature of higher order electric susceptibilities (*e.g.* the second order susceptibility of lithium niobate is around 10^{-12} V/m), the field of NLO only began after the advent of the laser in 1960 [12]. Despite the apparent paradox of combining high laser intensities with quantum processes at the few photon level, it was

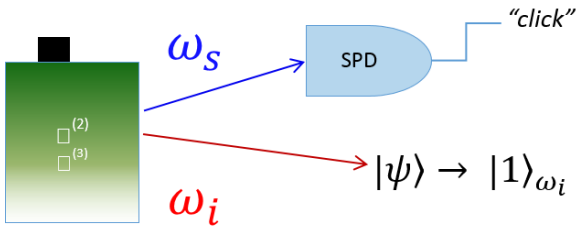

Figure 1.2: A schematic of a heralded single photon source, with the signal or herald photon being detected and projecting the idler photon into a single photon state.

realised within the decade that NLO provides a promising tool for exploring quantum optics, a typically low intensity affair.

NLO faces its own set of challenges as a basis for photon sources. Due to the very weak nature of higher order electric susceptibilities we must use relatively high intensity light to produce even a few photons, placing constraints on pump sources. Furthermore, this process is not deterministic – with any given pulse we do not know if we will produce any of the desired photons. However, as many nonlinear processes produce photons in pairs, we can use the detection of one photon as a *herald* of the other, counteracting their non-deterministic generation (see fig. 1.2). This introduces another issue – to preferentially generate single pairs of photons rather than higher order pairs, we must keep our laser intensities low, which limits the brightness of the source. Finally, we must deal with sources of noise. We cannot control every process occurring within our nonlinear materials that will produce spurious photons. Examples of such processes include spontaneous Raman scattering [13], fluorescence from chemical impurities (such as trace iron in glass [14]), and simple linear attenuation where we lose only a single photon. These losses tend to drive the photon statistics towards classical light, obviating their use for quantum experiments.

Most relevant to our discussion in this thesis is spontaneous Raman scattering, which is a well-understood phenomenon. When light of frequency ω is incident upon a medium, some photons are inelastically scattered such that their frequency is shifted by an amount $\Delta\omega_R$, so that photons at frequencies $\omega_{\mathrm{S,A}} = \omega \pm \Delta\omega_R$ are produced. The down-shift is known as the Stokes component, and the up-shift the anti-Stokes component. The Stokes process occurs when the photon causes an atom or molecule to transition from its ground state $|g\rangle$, to another state $|n\rangle$, via a virtual excited state $|n'\rangle$, associated with the emission of a phonon. The anti-Stokes process is similar, but the transition is from $|n\rangle$ to $|g\rangle$, and is typically weaker due to a low population of phonons at room temperature[15]. Both processes are illustrated in fig. 1.3. In crystals, which have regular structures, the Raman peaks are typically narrow – on the order of tens of terahertz. However, in amorphous materials such as glass, the Raman spectrum can be quite broad – on the order of hundreds of terahertz. As we will show later, this is often problematic.

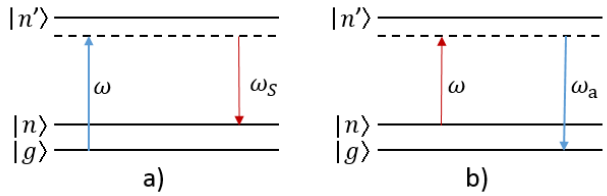

Figure 1.3: The energy levels involved with the spontaneous Raman process. a) The Stokes process. b) The anti-Stokes process.

1.3 Why use NLO sources?

In spite of these complications NLO offers some clear advantages over other systems. The first of these is the high rate at which these sources can produce photons (*e.g.*10^6 photons per second in a recent lithium niobate waveguide[16]). Furthermore, whilst NLO sources can be created with bulk optics, with large optical tables covered in mirrors, lenses and large chunks of crystals, they can also be achieved in fibre or integrated onto photonic chips. In 2005 Li *et al.* demonstrated the ability to generate polarisation-entangled photons in standard optical fibre in the 1550 nm telecom band [17]. They used these photons to demonstrate Hong-Ou-Mandel interference with greater than 90% visibility and to violate Bell's inequality. McMillan *et al.* (2009) took another approach, generating correlated photon pairs at 1570 nm in photonic crystal fibre [18]. Clark *et al.* demonstrated another photonic crystal fibre source in 2011, with the ability to tailor the spectral properties of the photons [19].

As for integrated photonic chips, the generation of correlated photon pairs has been demonstrated in chalcogenide glass waveguides [20], as well as in semiconductor nanowires on silicon photonic crystals [21]. Both of these schemes can be operated at room temperature in air, removing the need for large cooling and vacuum systems. Integration also leads to the possibility of hundreds, or even thousands of optical elements on a single chip – ideally forming entire devices, including both photon sources and detectors, ideal for quantum information processing. These photonic chips can be made to be extremely compact, as demonstrated in fig. 1.4. Other examples of on-chip sources include a SFWM source on a silica photonic chip by Spring *et al.* in 2013 [22]. This compactness leads to a scalability that is a strong motivator behind such research around the world, allowing for more commercial applications. Feeding into this, much of this technology is compatible with existing semiconductor electronics and fabrication capabilities. On top of this, there are also novel fabrication techniques available, such as the femtosecond laser direct writing technique used to fabricate a single photon source beyond 1100 nm in fused silica by Yan *et al.* in 2015 [23]. This technique can be extended to 3D waveguides, allowing for the design of more complex circuits.

The ability to integrate optical elements onto photonic chips has further advantages.

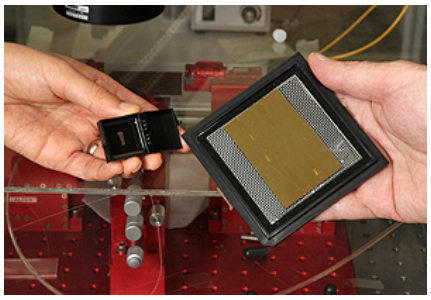

(a)

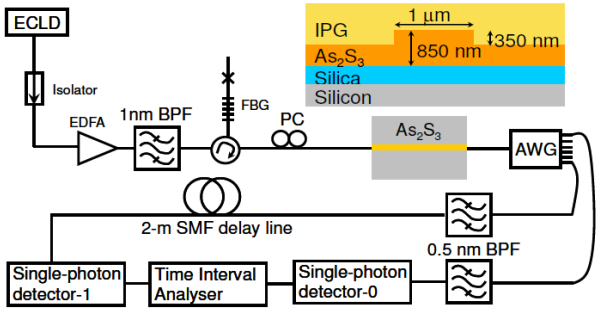

(b)

Figure 1.4: (a): An example of how small integrated photon sources can be: the newer packaged silicon chip on the left (which contains features only 100 μm long) compared to an older, centimetre scale nonlinear glass chip. (b): A schematic of the experiment in which this particular device was used, including a diagram of the glass chip itself. [24]

The use of waveguides allows for great control over how waves of different frequencies interact, in particular we can engineer a more desirable *dispersion relation*. This allows us to selectively *phasematch* which processes take place and which do not. We have this ability as the frequency conversion that takes place must approximately satisfy both the conservation of energy and momentum, the latter imposing conditions on the allowed combination of wavevectors. These waveguides can be designed to have tight mode confinement, leading to a greater nonlinear enhancement than would be possible in bulk materials.

Finally, integrated optical chips are solid-state devices. This gives them inherent stability as single photon sources, as they are less sensitive to environmental changes and will reliably reproduce indistinguishable photons. We can also attach such systems to thermal reservoirs, giving us temperature stability, or even thermal control. For example, in 2015 Carolan *et al.* demonstrated a reprogrammable optical circuit with 15 Mach-Zehnder interferometers and 30 thermo-optic phase shifters integrated onto a single photonic chip that could reproduce various states with a fidelity of 0.999 [25]. However, while the current state-of-the-art for quantum circuits involves dozens of elements integrated onto a chip, integrated sources are further behind.

1.3.1 Schemes for producing photons

At present there are two main techniques for producing pairs of photons by nonlinear optics: spontaneous parametric down conversion (SPDC), a second order process, and spontaneous four wave mixing, a third order process [26]. When performing SPDC we pump strongly at some frequency ω_p, and "spontaneously" generate *signal* and *idler* photons of lower frequencies, ω_s and ω_i. This is in contrast to the equivalent classical process, *difference-frequency generation*, where we must stimulate the process with a seed beam at ω_i. This is

because, at the single photon level, vacuum fluctuations stimulate the generation of the signal and idler photons. Formally, this is described by the two-mode squeezing operator

$$\hat{S}(\xi) = \mathrm{e}^{\xi \hat{a}^\dagger \hat{b}^\dagger - \xi^* \hat{a}\hat{b}} \tag{1.2}$$

acting on the vacuum state $|0,0\rangle$, as shown in fig. 1.5, where $\hat{a}^\dagger |0,0\rangle = |1,0\rangle$ and $\hat{b}^\dagger |0,0\rangle = |0,1\rangle$, and $\hat{a}^\dagger$, $\hat{b}^\dagger$ correspond to modes at the signal frequency ω_s, and idler frequency ω_i, with ξ containing the pump strength, nonlinear coefficient and time dependence. As previously discussed, this produces mostly vacuum, and a contribution to the single-pair state $|1,1\rangle$, but it also has a non-negligible likelihood of generating higher order pairs ($|n,n\rangle$, $n \geq 2$). These higher order pairs are problematic, as most quantum protocols rely on having only single photons present, and we do not yet have reliable (and affordable) number resolving photon detectors to remove them through real-time detection or post-selection.

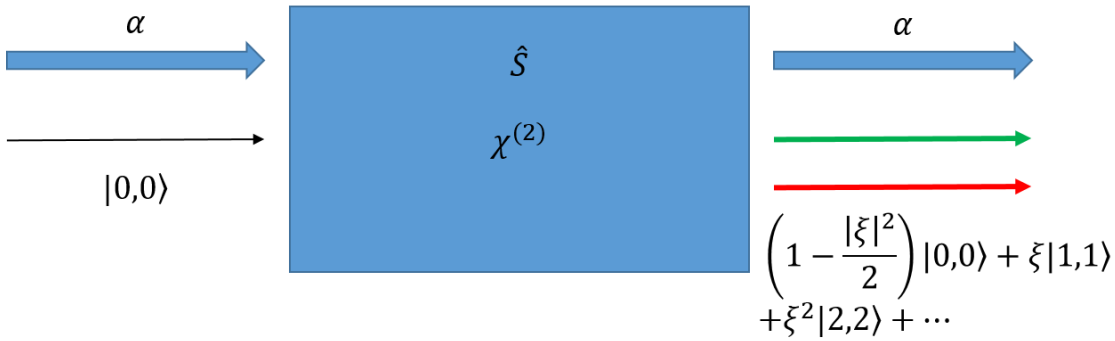

Figure 1.5: The input and output states when performing SPDC, demonstrating the effect of the squeezing operator on the vacuum state for small ξ. Here α is the amplitude of the classical pump.

For sufficiently small values of ξ the probability of generating at least the second order pair is proportional to $|\xi|^4$. This means that for low pump powers the probability of generating higher order pairs is low (but non-zero), although the rate of single pairs is correspondingly lower.

Spontaneous four wave mixing is a more complicated process than SPDC. As the name suggests there are now four fields interacting (plus a special case, degenerate SFWM where two of the fields have the same frequency), which leads to some effects not seen in SPDC through the $\chi^{(3)}$ nonlinearity including cross-phase modulation, self-phase modulation, free-carrier absorption and two photon absorption [27]. Similarly to SPDC, SFWM sources also generate higher order pairs. There is still interest in SFWM despite these extra effects, as every material has a third order nonlinear susceptibility, and it is possible to generate correlated photon pairs in a single spatial mode directly inside fibres. This means that they couple well into existing infrastructure [28]. However, due to the non-instantaneous molecular response

underlying the third order nonlinearity, many amorphous SFWM sources are plagued by the aforementioned spontaneous Raman scattering [29]. Even with tight filtering around the signal and idler frequencies, we see unwanted Raman photons being generated from the pump field in the form of uncorrelated single photons.

It is sometimes possible to reduce this problem by working in low Raman noise frequency windows, whether this is by using dispersion engineered waveguides or by selecting an appropriate material to use as a platform. This was demonstrated by Collins *et al.* in 2012 [30] through the use of careful dispersion engineering in a chalcogenide glass rib waveguide. They found that when performing SFWM for a TM mode, there was a region of low Raman noise when detuned from the pump by around 8 THz (see fig. 1.6).

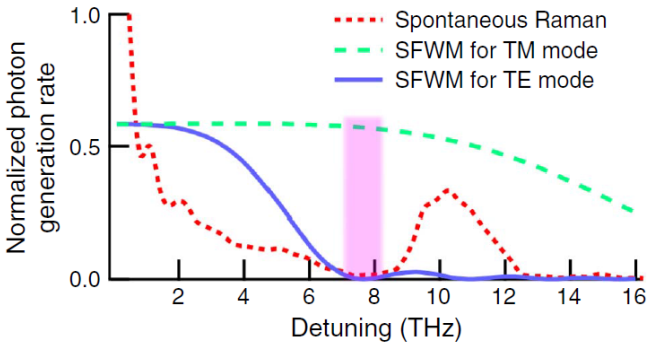

Figure 1.6: Finding a region of low spontaneous Raman noise while performing SFWM [30]. The signal to noise ratio is very good in the 7.5 THz − 8.5 THz band.

This constitutes a dramatic improvement in the standard signal to noise measure, the coincidence-to-accidental ratio (CAR), where a coincidence constitutes the detection of a correlated pair of photons. Here the CAR is defined as the ratio of the rate of correlated counts, C_{raw}, to the rate of noise counts, A, that is CAR $= C/A$ where the true coincidence rate is related to the measured ratio by $C = C_{\text{raw}} - A$. We can see this improvement in fig. 1.6, where the total coincidence rate is given in blue, the noise rate in red, and the true coincidences in green. In fig. 1.7.b, outside the low-noise window, there are more counts due to Raman scattering than from SFWM. In contrast, fig. 1.6.a shows that in the low-noise region, the true coincidence rate approaches the total coincidence rate. While promising, this solution does have stringent spectral and material requirements. Such convenient Raman-free windows are rare.

1.3.2 Multiplexing

Incidentally, the multiple pair generation problem would appear to limit the feasibility of both SPDC and SFWM as bright sources of single photons regardless of other noise issues. However, when we have high heralding efficiency (that is, when we have a single photon in the

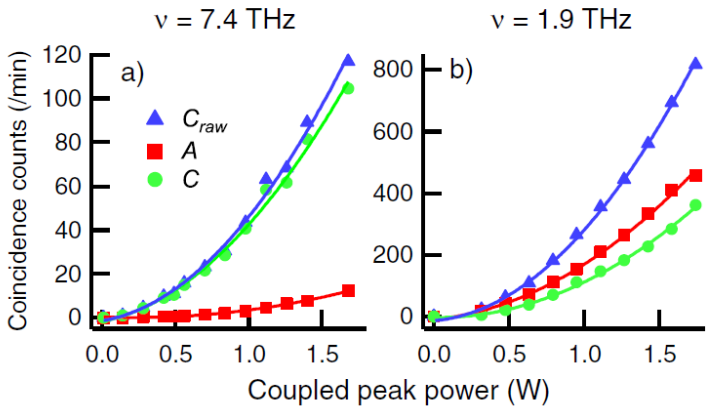

Figure 1.7: (a) In the low-noise region, the true coincidence rate (green) approaches the total coincidence rate (blue). (b) Outside the low-noise region, the noise rate (red) is comparable to the true coincidence rate [30].

signal arm, the herald arm's detector correctly fires a high percentage of the time), we can use multiplexing with multiple sources to increase the effective brightness of a source without introducing more undesirable states. This can be done with either spatial multiplexing, where we use multiple sources, or with temporal multiplexing, where we use delay lines to combine together multiple single pair events. In 2013 Collins *et al.* [31] demonstrated how multiplexing two SFWM integrated waveguide sources could lead to a 63% increase in the heralded photon rate, which is only slightly less than the expected enhancement with a lossless switch. In an ideal world, without detector ineffiencies and coupling losses, one would expect the rate to nearly double, *i.e.* a 100% increase in the rate [32]. To achieve the measured enhancement, as shown in fig. 1.8, the photons produced in each waveguide are separated by an arrayed waveguide grating, where they pass through separate arms. The idler photon goes into the herald arm with a single photon detector and the signal photon goes through a delay line (here a fibre loop). If the herald arm detector clicks, the delay line gives the electronic logic circuit time to control the optical switch which allows only the heralded photon through. The result is a heralded photon source with a higher rate, but with a reduction in the fraction of multiple pairs.

1.4 How do we characterise photon sources?

To improve sources, we must be able to measure and classify them. Here we describe a couple of important metrics.

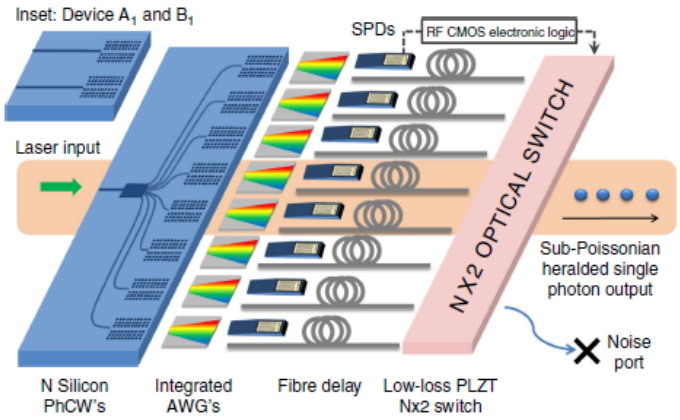

Figure 1.8: An example of the kind of device envisaged by Collins *et al.* in [31].

1.4.1 The second-order correlation function

An important measure for the "single-ness" of a source is the second order correlation function $g^{(2)}(\tau)$[26]. For a single mode, we write

$$g^{(2)}(\tau) = \frac{\left\langle \hat{a}^\dagger(t_1)\hat{a}^\dagger(t_2)\hat{a}(t_2)\hat{a}(t_1)\right\rangle}{\langle \hat{a}^\dagger(t_1)\hat{a}(t_1)\rangle \langle \hat{a}^\dagger(t_2)\hat{a}(t_2)\rangle} = \frac{\langle : I(t_1)I(t_2) : \rangle}{\langle I(t_1)\rangle \langle I(t_2)\rangle}, \tag{1.3}$$

where : _ : denotes normal ordering. This is a "normalised" measure of the likelihood of two photons arriving at their respective detectors with temporal separation τ. A value $g^{(2)}(0) = 1$ indicates that we have a coherent source, such as a laser. If we have $g^{(2)}(0) = 2$, then we have a thermal source (we see photon bunching as we would with a blackbody emitter). However, $g^{(2)}(0) = 0$ tells us that we have a true single photon source – our photons are anti-bunched, they arrive separately. For their multiplexed source, Collins *et al.* quote a value of $g^{(2)}(0) = 0.19 \pm 0.02$ [31], indicating that their source does indeed operate in the single-photon regime. Another convincing demonstration in a femtosecond laser direct written waveguide is given by Spring *et al*, showing $g^{(2)}(0) = 0.0092 \pm 0.0004$ for a pump power of 25 mW [22].

The form in eq. (1.3) is technically appropriate for truly single photon sources. For characterising heralded pair sources, a number of variations can be defined that distinguish correlations in the same channel from correlations between signal and idler channels [26, 33].

1.4.2 Correlations

When parametric sources generate photon pairs it is often the case that there are correlations between the photons produced, such as in polarisation, or frequency. If we limit ourselves to the discussion of frequency correlations, in analogy to eq. (1.1) we can represent the photon

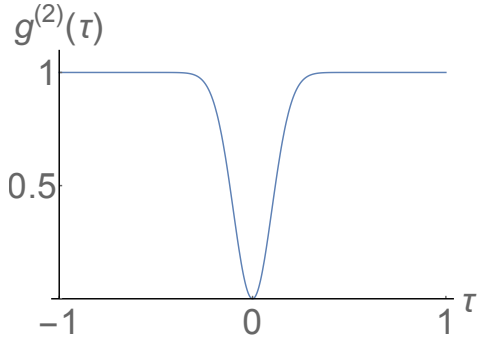

Figure 1.9: A sketch of an idealised second order correlation function, $g^{(2)}(\tau)$, for a single photon source.

pair state as

$$|\psi\rangle = \int_0^\infty \mathrm{d}\omega_1 \int_0^\infty \mathrm{d}\omega_2 \, \phi(\omega_1, \omega_2) \, \hat{a}^\dagger_{\omega_1} \hat{a}^\dagger_{\omega_2} |\mathrm{vac}\rangle, \tag{1.4}$$

where the complex function ϕ is the *joint spectral amplitude* (JSA). In essence, this is the wave function for the joint photon (or "biphoton") state. It describes the probability of a pair of photons being generated in the interval $\mathrm{d}\omega_1 \, \mathrm{d}\omega_2$, thus it plays an important role when designing photon sources.

The shape of the JSA contains information about the spectral correlations between the two photons. For example, the function in fig. 1.10a can be written as $\phi(\omega_1, \omega_2) = f(\omega_1)g(\omega_2)$. This means that the state is separable, or uncorrelated. The same is not true of figs. 1.10b to 1.10d, meaning that they describe the generation of correlated photon pairs.

We can distinguish between correlated and uncorrelated states by finding the *Schmidt number*, which is a measure of the number of independent uncorrelated frequency modes making up the state. We find the Schmidt number K, by taking the *Schmidt decomposition* of the JSA. It is a basic result of linear algebra that any complex function of two variables, $F(x, y)$, can be represented as a sum over the product of two families of single variable functions each of which form complete orthonormal sets.

More succinctly, this means $F(x, y) = \sum_\lambda \sqrt{p_\lambda} f_\lambda(x) g_\lambda(y)$ for some constant coefficients p_λ satisfying $\sum_\lambda p_\lambda = 1$. As shown in fig. 1.10d, this very loosely could be thought of as being able to write any two variable function as a direct sum of "circle" states like the one seen in fig. 1.10a. This is a continuous analogue of the singular value decomposition of a matrix. The Schmidt number $K = \sum_\lambda 1/p_\lambda^2$ then is a measure of how many non-zero coefficients are required, and we note that $K \geq 1$. A state is said to have no correlations, or be *separable*, if $K = 1$. This would mean $\phi(\omega_1, \omega_2) = \Phi(\omega_1)\Phi(\omega_2)$, corresponding to fig. 1.10a. If $K > 1$ then there are spectral correlations between the two photons, as shown in fig. 1.10b. The Schmidt decomposition is a complete characterisation of entanglement of a biphoton [34]. In general this is not possible for $n \geq 3$ photons, as no analogous decomposition is known.

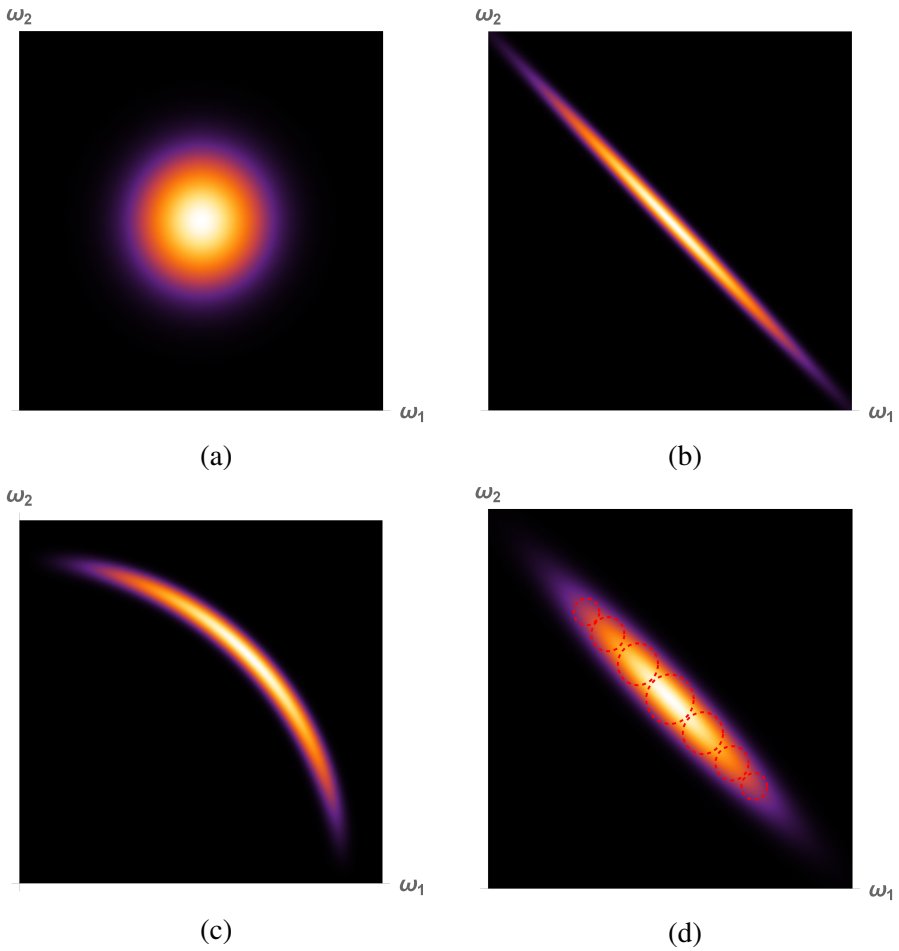

Figure 1.10: Plots of the normalised joint spectral intensity $|\phi|^2$. (a): A factorable or separable biphoton function. (b): A non-factorable biphoton function. (c): An example of the effects of strong dispersion on the joint spectral amplitude. (d): An illustration of approximately how many Schmidt functions we need to represent our state, loosely indicated by the dashed circles.

1.4.3 Factorable or not?

While there are experiments that take advantage of correlated sources, most quantum protocols devised to date require pure states. As such, we must understand whether or not a heralded source is producing separable states, as when we measure the herald photon the remaining idler photon is projected into a single photon state. As our detectors do not have perfect frequency resolution this will necessarily introduce some classical uncertainty to the single photon's frequency. This leads to a density operator $\hat{\rho}$ for the state which is not pure. If we consider a correlated biphoton state, when we measure with wide spectral filters we lose the ability to distinguish the frequency of our pairs, as illustrated in fig. 1.11a. To counter this we can tightly filter our detectors, as shown in fig. 1.11b, and recover a highly pure state. However, this will decrease the rate of coincidences. Ideally we would work with a factorable or uncorrelated biphoton state as seen in fig. 1.11c. Then, it does not matter how broad or

narrow the filtering is, the result will be a pure state.

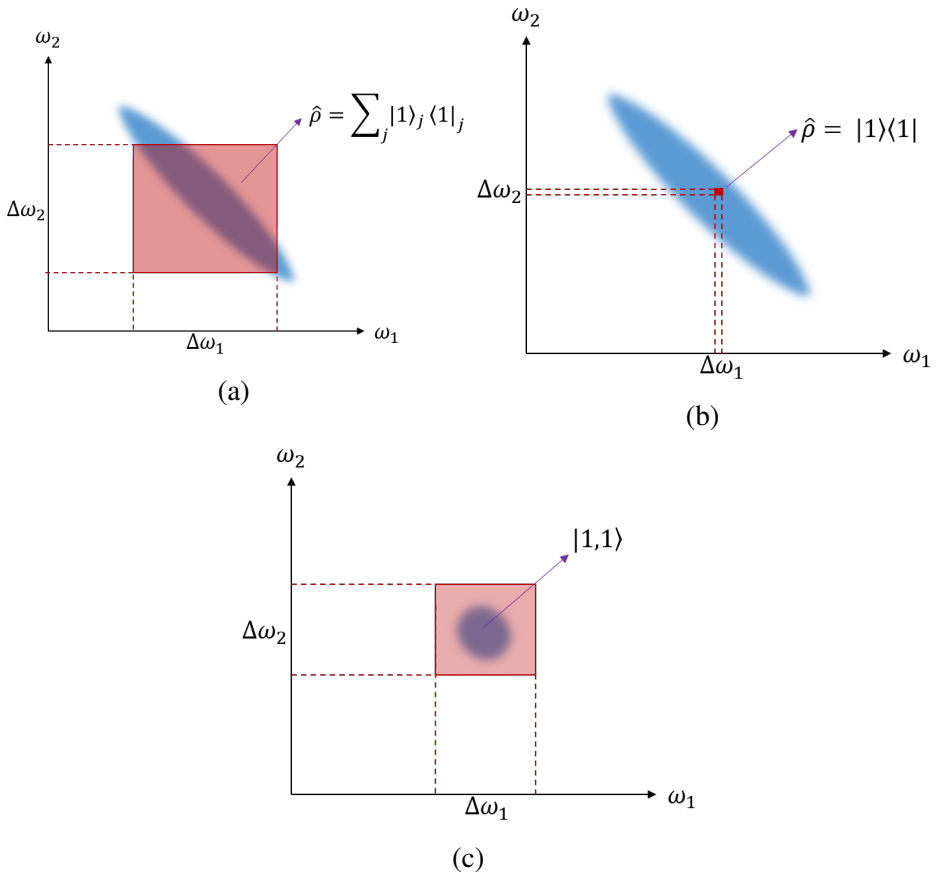

Figure 1.11: (a): Taking measurements with wide spectral filters of a correlated biphoton state results in a mixed state as described by the density operator, $\hat{\rho}$. (b): Using narrow filtering when measuring a correlated biphoton state yields a pure state, at the price of a lower rate. (c): Even when using wide filters when measuring an uncorrelated or factorable biphoton state, the result is a pure state.

1.5 Other $\chi^{(3)}$ processes

There is another process which has generated some interest, which will become relevant to our discussion in chapter 2, that involves producing photon triplets, known as third order spontaneous parametric down conversion (TOSPDC). Classically this process is known as *one-third harmonic generation*, with its inverse process *third harmonic generation* (OTHG and THG respectively) being more commonly known. In the single-photon regime, a pump photon at the frequency ω spontaneously fissions into three photons at $\omega/3$. This process can be difficult to phase match [35], but in principle high conversion efficiency can be achieved. As a result, a popular alternative is to use cascaded processes to achieve a similar result [36]. Ultimately however the rate of triple photons is incredibly low when the process is not seeded, on the order of 0.01 triplets per day, or around 11 events per PhD student [37]. Whilst it

is possible to seed TOSPDC to generate photon triplets at a more useful rate, it becomes difficult to distinguish the triplets from the seed fields [37]. However as we will see, the idea of seeding a three photon down conversion process does present a potential solution to the problem of spontaneous Raman scattering.

We have seen that there are a number of problems to be addressed if we are to reliably produce single photons on demand, using nonlinear optical techniques. We need bright sources, whilst simultaneously limiting the production of higher order pairs. We need to control the correlations between the pairs produced by our devices. Ideally, these devices would be easily scalable. Finally, we must limit sources of noise, particularly when working with the amorphous materials that make up a significant fraction of modern optics. While tackling all of these problems is far beyond the scope of this thesis, it is our intention to discuss a potential solution the problem of spontaneous Raman scattering.

I'm smart enough to know that
I'm dumb.

Richard Feynman

2

A New Way

Many of the most commonly used platforms for optics are based on amorphous materials, such as fused silica glass (for example, in optical fibres). Unlike crystalline materials, amorphous materials exhibit broadband spontaneous Raman scattering. This is the result of inhomogeneous broadening – unlike the uniform environment of a regular lattice, in an amorphous material, each oscillator has a different environment and experiences different electromagnetic fields, and responds differently. Consequently, the photons emitted by spontaneous Raman scattering have a broad energy range, and contaminate a large part of the photon pair spectrum. In contrast, in crystalline materials the Raman emission is narrow, and one can simply choose to filter out photon pairs in the Raman window. Having established that this is a key source of noise that must be overcome in single photon sources, the purpose of this project is to propose a new third order process for generating correlated photon pairs that is less vulnerable to Raman noise. In this chapter we begin to describe this process, verify that it can be phasematched, and confirm that it will produce the pairs of photons we desire for a heralded single photon source.

2.1 An introduction to Stimulated Spontaneous Three Photon Down Conversion

Consider the following set up. Similarly to TOSPDC discussed in section 1.5, we pump a $\chi^{(3)}$ material strongly at the third harmonic ω_p (α_4 in fig. 3.3), and one pump photon is down-converted to three photons around the fundamental frequency, ω_s. However, by adding a seed beam coinciding with the frequency of one of the triplet of photons (α_3^*), we stimulate the production of pairs around ω_s ($\hat{a}_1^\dagger$ and $\hat{a}_2^\dagger$). We call this process Stimulated Spontaneous Three Photon Down Conversion (SSTPDC).

One advantage of this process is that the Stokes band (with a bandwidth on the order of $\Delta\nu_R = 10\,\text{THz}$) sits in between the higher frequency photon of the pair and the pump (as demonstrated in fig. 3.3), which are separated by $\Delta\nu_{\text{SSTPDC}} \approx 100\,\text{THz}$. This means that the overlap with the pair is much smaller than it would be for the equivalent SFWM process (illustrated in fig. 2.2). As the seed itself is weak, it does not contribute strongly to spontaneous Raman scattering.

SSTPDC also gives us more flexibility in what lasers we use to produce our single photons. For example, if one has a high power short pulse frequency doubled Nd:YAG laser at 532 nm, then one can produce photon pairs near the 1550 nm band with only a weak laser diode seed. If we are working from a single source, all pulse properties are determined by that one source. However, if we work with two sources, we have an extra degree of freedom (for example, we could choose different pulse durations).

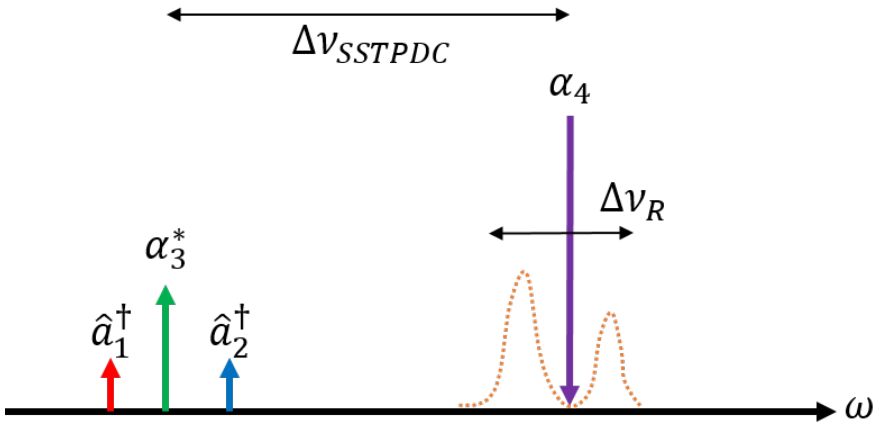

Figure 2.1: A schematic of the frequencies involved in SSTPDC and the Raman side bands generated around the pump. Spacings are not to scale.

Adequately describing this process is not straightforward. By design, SSTPDC takes place across a broad frequency range. We are operating with multiple frequencies in the multimode regime, with very short pulses, and there are several nonlinear processes taking place at the same time. These include self-phase modulation and cross-phase modulation, as

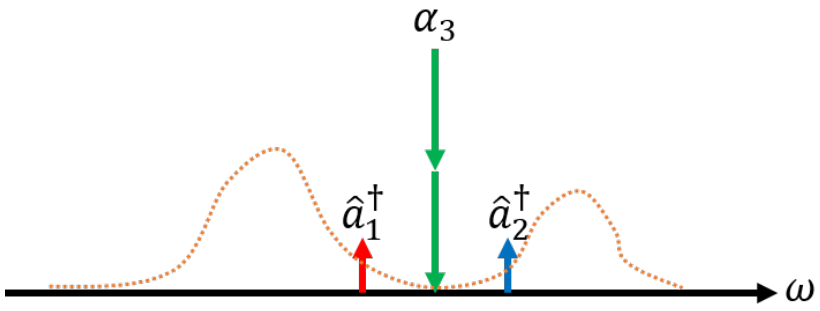

Figure 2.2: A schematic of the frequencies involved in degenerate SFWM, including the Raman side bands generated around the pump.

well as the Raman effect we are seeking to mitigate. Due to the requirements of tight spatial confinement, we must also use a description that encompasses waveguides.

2.1.1 Program of work

In this thesis, we will first establish that it is possible to phasematch SSTPDC by analogue with its classical counterpart, in chapter 2, section 2.2. This will allow us to consider the contributions of self and cross phase modulation, something not considered in the quantum treatment here due to its small effect versus the added complexity. Then in section 2.3, we will develop a simple few-mode model to establish that SSTPDC does indeed produce pairs, and we can incorporate the Raman impact on pair production. In chapter 3, section 3.1 we establish the nonlinear Hamiltonian that fully incorporates the full multi-frequency and multimode nature of SSTPDC, as well as the effects of dispersion. After moving into the interaction picture in section 3.3, we examine the first order solution to the Schrödinger equation in section 3.4. This allows us to both determine a rate of pair production in chapter 4, and the nature of the *joint spectral intensity* (JSI), the absolute value squared of the joint spectral amplitude.

2.2 A classical interlude

With short, energetic pulses, the effects of self and cross phase modulation play an important role in phasematching considerations. However, in the full Hamiltonian formalism we adopt in chapter 3, there is additional complexity in incorporating these nonlinear contributions to the phasematching. As such, we will rely on a classical analogue to establish the full phasematching conditions.

For the classical four wave mixing process, we pump some $\chi^{(3)}$ material at the third harmonic, ω_p, add a seed probe at the fundamental frequency ω_s, and produce two new fields at ω_1 and ω_2 (as this is a classical process, at least one of these two fields are also weakly

seeded). Rather than being governed by the Schrödinger equation, now we must satisfy the nonlinear electromagnetic wave equation:

$$\nabla \times \nabla \times \mathbf{E}(\mathbf{r}, t) + \frac{n^2}{c^2}\frac{\partial^2}{\partial t^2}\mathbf{E}(\mathbf{r}, t) = -\mu_0 \frac{\partial^2}{\partial t^2}\mathbf{P}_{\mathrm{NL}}(\mathbf{r}, t) \tag{2.1}$$

where c is the speed of light in a vacuum, μ_0 is the vacuum permeability, $\mathbf{E}(\mathbf{r}, t)$ is the electric field, and

$$\mathbf{P}_{\mathrm{NL}}(\mathbf{r}, t) = \epsilon_0 \left(\chi^{(2)}\mathbf{E}^2(\mathbf{r}, t) + \chi^{(3)}\mathbf{E}^3(\mathbf{r}, t) + \dots \right)$$

is the nonlinear polarisation. For our purposes, it suffices to consider a single polarisation to treat $\mathbf{E}(\mathbf{r}, t)$ as scalar, and only the third order nonlinear polarisation, and we will account for dispersion later. Then, in the weak guidance regime where Δn is small, our wave equation is

$$\nabla^2 E(\mathbf{r}, t) - \frac{n^2}{c^2}\frac{\partial^2}{\partial t^2}E(\mathbf{r}, t) = \frac{1}{c^2}\chi^{(3)}\frac{\partial^2}{\partial t^2}E^3(\mathbf{r}, t). \tag{2.2}$$

To transform this into an expression involving slowly varying amplitudes, we write the electric field as

$$E(\mathbf{r}, t) = \frac{1}{2}\sum_{j=1}^{4}\left(a_j(z, t) f_j(x, y) \mathrm{e}^{i(\beta_j z - \omega_j t)} + \mathrm{c.c.} \right), \tag{2.3}$$

where the sum is over modes, $a_j(z, t)$ are the longitudinal amplitudes, $f_j(x, y)$ are the solutions to the modal wave equation, β_j and ω_j the propagation constants and angular frequencies for each mode. We will take $j = 1, 2$ as the signal and idler bands, and $j = 3, 4$ as the seed and pump bands, respectively.

Here, we follow the standard procedure for finding the coupled mode equations. Firstly, we assume that the amplitudes involved vary sufficiently slowly that their second derivatives are negligible. As the nonlinearity is small, all derivatives of amplitudes associated with nonlinear terms may also be taken as negligible. Then, examining only one wave at a time, we remove terms associated with solutions to the linear wave equation, identifying group velocities and effective coupling areas.

This allows us to extract four coupled equations, one for each field (where ω_4 corresponds to the pump, ω_3 the seed, and ω_1, ω_2 the signal and idler). These equations of motion have

the form

$$\begin{aligned} i\partial_z b_j(z,t) + \frac{i}{v_g(\omega_j)}\partial_t b_j(z,t) =& \frac{3\chi^{(3)}\omega_j^2 \left|b_j(z,t)\right|^2 b_j(z,t)}{8c^2\beta_j A_{jjjj}} \\ &+ \frac{3\chi^{(3)}\omega_j^2}{4c^2\beta_j}\sum_{i=k}^{m}\left[\frac{|b_k(z,t)|^2}{A_{jiji}}\right] b_j(z,t) \\ &+ \frac{3\,\mathrm{e}^{q(j)i(\beta_4-\beta_3-\beta_2-\beta_1)z}\chi^{(3)}\omega_j^2 b_m(z,t)b_l^*(z,t)b_k^*(z,t)}{4c^2\beta_j A_{jklm}}, \end{aligned} \tag{2.4}$$

where $b_i(z,t) = a_i(z,t)\int \mathrm{d}x \int \mathrm{d}y\ |f_i(x,y)|^2$ are rescaled field amplitudes, the sum is performed over the indices k, l, m, the equation for each $b_i(z,t)$ is given by a cyclic permutation of $(j,l,m,k) = (1,2,3,4)$, and with $q(j=4) = 1$, otherwise $q(j) = -1$. Additionally

$$A_{ijlm} = \frac{\sqrt{\int \mathrm{d}x\,\mathrm{d}y\,|f_i(x,y)|^2 \int \mathrm{d}x\,\mathrm{d}y\left|f_j(x,y)\right|^2 \int \mathrm{d}x\,\mathrm{d}y\,|f_l(x,y)|^2 \int \mathrm{d}x\,\mathrm{d}y\,|f_m(x,y)|^2}}{\int \mathrm{d}x\,\mathrm{d}y\, f_i(x,y) f_j(x,y) f_l^*(x,y) f_m^*(x,y)}$$

are the effective mode coupling areas, and $v_g(\omega)$ are the group velocities for a given frequency. The first term on the right hand side of eq. (2.4) is the self-phase modulation, the next three in the sum describe cross-phase modulation with each field, and the final term is the four wave mixing term.

As we are primarily interested in the feasibility of phasematching this process, rather than resorting to numerics, we shall move into the undepleted pump regime and proceed analytically. First, we assume that all mode overlaps are approximately equal, so that $A_{ijkl} = A_{\mathrm{eff}}$. Then we introduce the classical nonlinear parameter,

$$\gamma_i = \frac{3\chi^{(3)}\omega_i^2}{8c^2 A_{\mathrm{eff}}\beta_i},$$

and move to a quasi-continuous wave regime such that $\partial_t b_i = 0$. The equation of motion for the pump reduces to

$$i\partial_z b_4(z) - \gamma_4 |b_4(z)|^2 b_4(z) = 0.$$

In the undepleted pump approximation, $|b_4(z)|^2$ is constant, so the solution to this is

$$b_4(z) = b_{4,0}\,\mathrm{e}^{-i\gamma_4 |b_{4,0}|^2 z},$$

where $b_{4,0} = b_4(0)$. The absolute value squared of the amplitude is closely related to the power, but not equivalent. The correct relation for the power, obtained from the Poynting

vector, is

$$P_4(z) = \frac{c\, n_4 \epsilon_0}{4A_{\text{eff}}} b_4(z) b_4^*(z) = \frac{c\, n_4 \epsilon_0}{4A_{\text{eff}}} |b_{4,0}|^2 . \tag{2.5}$$

For the seed, signal and idler equations of motion, due to their small amplitudes, we disregard any terms that do not contain a pump amplitude. This leaves us with three coupled nonlinear equations,

$$i\partial_z b_3(z) - 2b_{4,0}\gamma_3 \, \mathrm{e}^{i(\Delta\beta - 4\gamma_4 P_4 A_{\text{eff}}/cn_4\epsilon_0)z} b_1^*(z) b_2^*(z) - \frac{8\gamma_3 P_4 A_{\text{eff}}}{c\, n_4 \epsilon_0} b_3(z) = 0, \tag{2.6}$$

$$i\partial_z b_2(z) - 2b_{4,0}\gamma_2 \, \mathrm{e}^{i(\Delta\beta - 4\gamma_4 P_4 A_{\text{eff}}/cn_4\epsilon_0)z} b_1^*(z) b_3^*(z) - \frac{8\gamma_2 P_4 A_{\text{eff}}}{c\, n_4 \epsilon_0} b_2(z) = 0, \tag{2.7}$$

$$i\partial_z b_1(z) - 2b_{4,0}\gamma_1 \, \mathrm{e}^{i(\Delta\beta - 4\gamma_4 P_4 A_{\text{eff}}/cn_4\epsilon_0)z} b_2^*(z) b_3^*(z) - \frac{8\gamma_1 P_4 A_{\text{eff}}}{c\, n_4 \epsilon_0} b_1(z) = 0, \tag{2.8}$$

where $\Delta\beta = \beta_4 - \beta_3 - \beta_2 - \beta_1$. To solve eqs. (2.6) to (2.8), we first introduce new fields $c_i(z) = b_i(z)\, \mathrm{e}^{8i\gamma_i P_4 A_{\text{eff}}/(c\, n_4 \epsilon_0)z}$ to remove the cross-phase modulation terms (the last term in each equation). We also introduce $\Gamma = -\frac{4P_4 A_{\text{eff}}}{cn_4\epsilon_0}\,(\gamma_4 - 2\gamma_3 - 2\gamma_2 - 2\gamma_1)$, giving

$$i\partial_z c_3(z) - 2\gamma_3 c_4(0) \mathrm{e}^{i(\Delta\beta+\Gamma)z} c_1^*(z) c_2^*(z) = 0, \tag{2.9}$$

$$i\partial_z c_2(z) - 2\gamma_2 c_4(0) \mathrm{e}^{i(\Delta\beta+\Gamma)z} c_1^*(z) c_3^*(z) = 0, \tag{2.10}$$

$$i\partial_z c_1(z) - 2\gamma_1 c_4(0) \mathrm{e}^{i(\Delta\beta+\Gamma)z} c_2^*(z) c_3^*(z) = 0. \tag{2.11}$$

Unfortunately, eqs. (2.9) to (2.11) are still coupled in a fashion that makes them difficult to solve. However, over short interaction lengths, the seed $c_3(z)$ is effectively constant with respect to $c_1(z)$ and $c_2(z)$. This is essentially an undepleted seed approximation. This allows us to replace $c_3(z)$ with its initial value, $c_3(0)$. So finally, we have two coupled equations

$$i\partial_z c_2(z) - 2\gamma_2 c_3^*(0) c_4(0) \mathrm{e}^{i(\Delta\beta+\Gamma)z} c_1^*(z) = 0, \tag{2.12}$$

$$i\partial_z c_1(z) - 2\gamma_1 c_3^*(0) c_4(0) \mathrm{e}^{i(\Delta\beta+\Gamma)z} c_2^*(z) = 0. \tag{2.13}$$

Approximating $\gamma_2 \approx \gamma_1 \approx \gamma_s$ (a reasonable approximation when the signal and idler frequencies are not far from the fundamental frequency), and identifying P_3 and P_4 through

$$\sqrt{\frac{16A_{\text{eff}}^2 P_3 P_4}{c^2 \epsilon_0^2 n_3 n_4}} \equiv c_3^*(0) c_4(0),$$

we find that eqs. (2.12) and (2.13) equations are nearly identical to the standard equations for

four wave mixing [38]. We thus identify the solutions

$$c_2(z) = (A_2 e^{gz} + B_2 e^{-gz})\, e^{i\kappa z/2}, \tag{2.14}$$

$$c_1(z) = (A_1 e^{gz} + B_1 e^{-gz})\, e^{i\kappa z/2}, \tag{2.15}$$

where A_i and B_i are determined by the boundary conditions, and $\kappa = \Delta k + \Gamma$. The parametric gain is given by

$$g = \sqrt{\frac{64\gamma_s^2 A_{\text{eff}} P_3 P_4}{c^2 \epsilon_0^2 n_3 n_4} - \left(\frac{\kappa}{2}\right)^2}.$$

In the case when the idler is not seeded ($c_2(0) = 0$), these solutions become

$$c_2(z) = 2iC_0\, c_1(0) \sinh(gz) e^{i\kappa z/2}, \tag{2.16}$$

$$c_1(z) = c_1(0) \left[\cosh(gz) + \frac{i\kappa}{2g} \sinh(gz)\right] e^{i\kappa z/2}, \tag{2.17}$$

where $C_0 = \gamma_s \sqrt{16 A_{\text{eff}}^2 P_3 P_4 / (c^2 \epsilon_0^2 n_3 n_4)}/g$. Translating these field amplitudes into powers, we find

$$P_2(z) = P_1(0) \left[1 + \frac{\kappa^2}{4|g|^2}\right] |\sinh(gz)|^2, \tag{2.18}$$

$$P_1(z) = P_1(0) \left\{1 + \left[1 + \frac{\kappa^2}{4|g|^2}\right]\right\} |\sinh(gz)|^2 . \tag{2.19}$$

In the limit when the parametric gain is small (*i.e.* $|\kappa| \gg 4\left|\gamma_s \sqrt{A_{\text{eff}} P_3 P_4 / (c^2 \epsilon_0^2 n_3 n_4)}\right|$ or $g \approx i\kappa/2$), the idler reduces to

$$\frac{P_2(L)}{P_1(0)} \approx \frac{8\gamma_s^2 A_{\text{eff}} P_3 P_4}{c^2 \epsilon_0^2 n_3 n_4} \text{sinc}^2\left(\frac{\kappa L}{2}\right) \tag{2.20}$$

Using the quantities defined in table 2.1, derived from the model developed in chapter 4, when the effect of self and cross-phase modulation is small, we demonstrate that the approximation made above is justified. In fig. 2.3 we plot a normalised $P_2(L)$ from eq. (2.18) and in fig. 2.4a $P_2(L)/P_1(0)$ from eq. (2.20). Note how they are essentially identical. If we increase the pump power to 1 MW, however, the results from eq. (2.18) look quite different (see fig. 2.4b). The system enters a regime where the nonlinear contributions to the phasematching from self and cross phase modulation are apparent. With the goal of producing only pairs of photons, an experiment is unlikely to enter this regime – but it is an effect worth considering.

Table 2.1: The parameters for the classical four wave mixing simulation.

Quantity	Symbol	Value
Refractive index	n_3	1.46
	n_4	1.44
Effective area	A_{eff}	$11.9\,\mu\text{m}^2$
Third order susceptibility	$\chi^{(3)}$	$3.8 \times 10^{-34}\text{m}^2/\text{V}^2$
Interaction length	L	3 mm
Group index	$n_g(\omega_s)$	1.426
	$n_g(\omega_p)$	1.613
Group velocity dispersion	$\beta_2(\omega_s)$	$-170\,\text{ps}^2/\text{km}$
	$\beta_2(\omega_p)$	$850\,\text{ps}^2/\text{km}$
Power	P_3	1 kW
	P_4	0.1 MW
Wavelength	λ_3	1550 nm
	λ_4	1550/3 nm

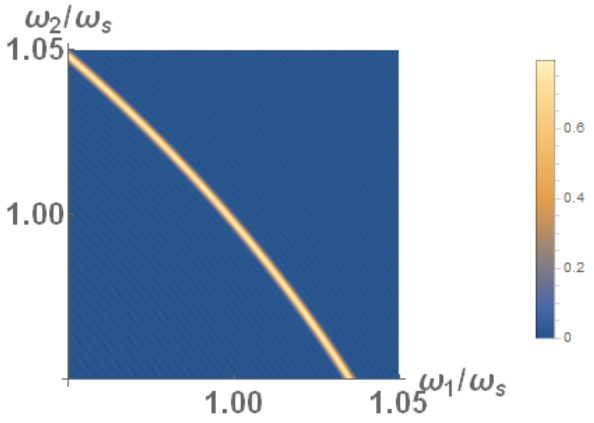

Figure 2.3: The idler field $P_2(L)$ plotted over a range of frequencies.

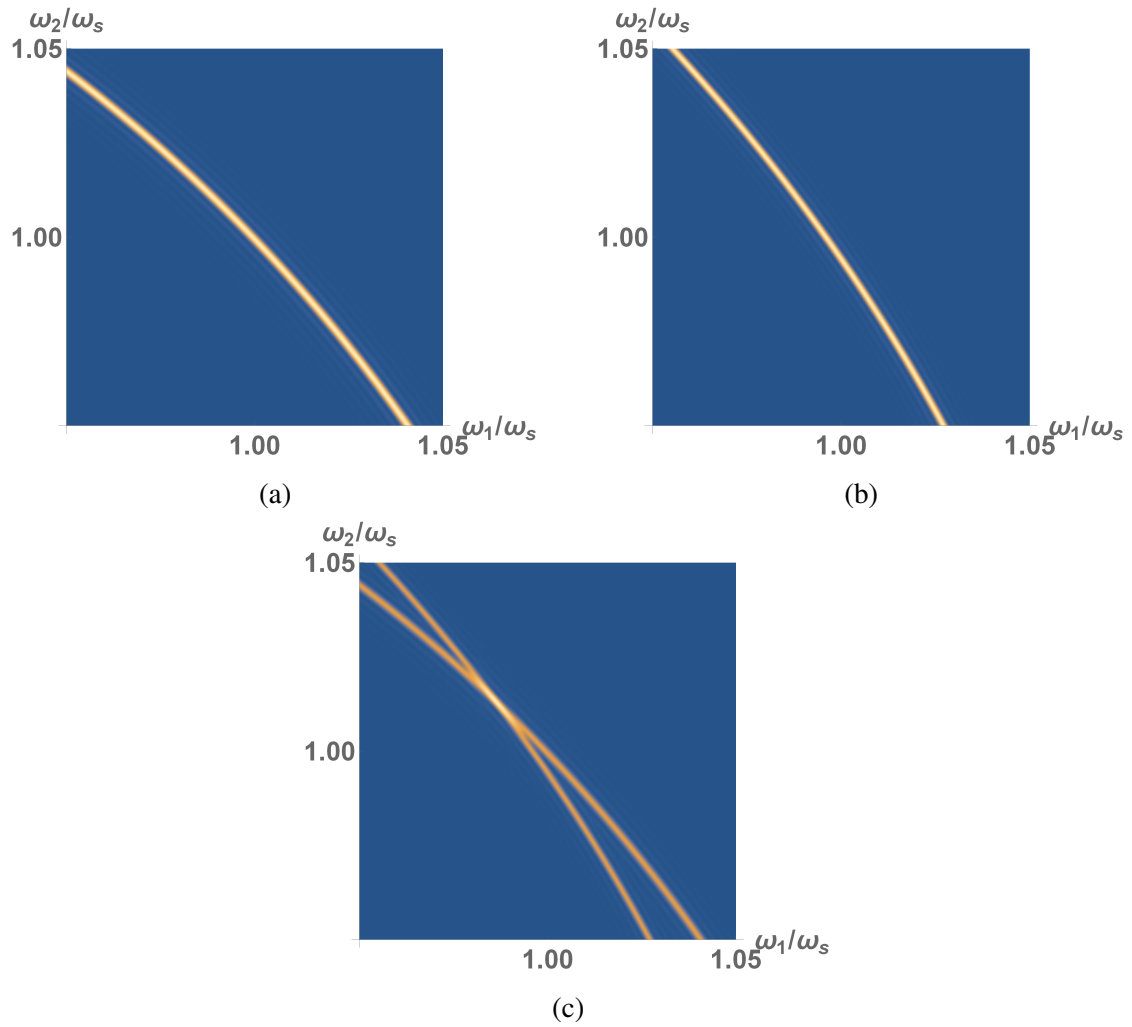

Figure 2.4: (a):The classical phasematching function, $\text{sinc}^2(\kappa L/2)$, where here the nonlinear contribution to the phasematching is negligible. (b): The classical phasematching function, $\text{sinc}^2(\kappa L/2)$, pumped with 1 MW to enter a regime where the nonlinear contribution to the phasematching is significant. (c): The sum of (a) and (b), showing the effect of self and cross phase modulation on the phasematching.

2.2.1 Observation

This four wave mixing process where we down convert the pump at the third harmonic to the fundamental frequency, and seed the production of signal and idler fields is similar to parametric gain. Therefore we can expect a similar analogue between SSTPDC and standard SFWM in the spontaneous regime.

2.3 A phenomenological approach to SSTPDC

2.3.1 Producing pair states

Now that we have seen this process can proceed at least classically, we try to develop intuition for the quantum process with a simple single mode Hamiltonian formulation, ignoring the short pulses involved. The seed and pump fields, $\hat{a}_3$ and $\hat{a}_4$, are strong coherent laser fields, which we will denote by their mean values α_3 and α_4. The signal and idler photons are then associated with operators $\hat{a}_1$ and $\hat{a}_2$. The process down-converts the pump field to produce the triplet, and one of these photons will coincide with the seed field. Ignoring self and cross phase modulation, the form of this Hamiltonian must be

$$\hat{H}_{\mathrm{I}} = \hbar\gamma\left(\alpha_3^*\alpha_4\hat{a}_1^\dagger\hat{a}_2^\dagger + \alpha_3\alpha_4^*\hat{a}_1\hat{a}_2\right), \tag{2.21}$$

where γ is the effective third order nonlinearity, and $\alpha_3^*\alpha_4\hat{a}_1^\dagger\hat{a}_2^\dagger$ corresponds to the mechanism described above. We note that α_3^* corresponds to energy being added to the seed field – because one of the down-converted pump photons contributes to the energy of this field.

To make life easier, we let $\alpha_j = \left|\alpha_j\right| \mathrm{e}^{i\phi_j}$, $\Delta\phi \equiv \phi_4 - \phi_3$ which is the relative phase between the two fields, and let $\Gamma = \gamma\,|\alpha_3|\,|\alpha_4|$. Now we have something more palatable:

$$\hat{H}_{\mathrm{I}} = \hbar\Gamma\left(\mathrm{e}^{i\Delta\phi}\hat{a}_1^\dagger\hat{a}_2^\dagger + \mathrm{e}^{-i\Delta\phi}\hat{a}_1\hat{a}_2\right). \tag{2.22}$$

The formal solution to Schrödinger's equation is given by

$$|\psi(t)\rangle = U_{\mathrm{I}}(t)\,|\psi(0)\rangle,$$

where $U_{\mathrm{I}}(t)$ is the time evolution operator. As our Hamiltonian does not have explicit time dependence, this is

$$\begin{aligned} U_{\mathrm{I}}(t) &= \mathrm{e}^{-i\hat{H}_{\mathrm{I}}t/\hbar} \\ &= \exp\left(-i\Gamma\mathrm{e}^{i\Delta\phi}t\hat{a}_1^\dagger\hat{a}_2^\dagger - i\Gamma\mathrm{e}^{-\Delta\phi}t\hat{a}_1\hat{a}_2\right) \\ &= \mathrm{e}^{\xi\hat{a}_1^\dagger\hat{a}_2^\dagger - \xi^*\hat{a}_1\hat{a}_2} \end{aligned} \tag{2.23}$$

where $\xi = -i\Gamma\mathrm{e}^{i\Delta\phi}t$. It is worthwhile to note that this is the same form as the two-mode squeezing operator (see eq. (1.2)). We could proceed to recover squeezing variances and parametric gain, but with an interest in pair generation, it is more fruitful to look at the states being generated with a vacuum input by expanding eq. (2.23) in ξ. This means that if

$|\psi(0)\rangle = |\text{vac}\rangle$ and ξ is small, we discover

$$\begin{aligned} e^{\xi \hat{a}_1^\dagger \hat{a}_2^\dagger - \xi^* \hat{a}_1 \hat{a}_2} |\text{vac}\rangle &\approx |\text{vac}\rangle + \xi \hat{a}_1^\dagger \hat{a}_2^\dagger |\text{vac}\rangle \\ &\quad - \frac{|\xi|^2}{2} \hat{a}_1 \hat{a}_2 \hat{a}_1^\dagger \hat{a}_2^\dagger |\text{vac}\rangle + \frac{\xi^2}{2} \left(\hat{a}_1^\dagger \hat{a}_2^\dagger\right)^2 |\text{vac}\rangle + \dots \\ &= \left(1 - \frac{|\xi|^2}{2}\right) |\text{vac}\rangle + \xi |1,1\rangle + \xi^2 |2,2\rangle + \dots \end{aligned} \tag{2.24}$$

This is precisely what we saw in fig. 1.5 As expected, we see single pairs being produced, as well as higher order pairs. We note that in order for this state to remain normalised, the coefficient of the vacuum term is no longer one [39].

2.3.2 Producing pair states with Raman noise

One of the expected features of SSTPDC is the ability to limit Raman noise by having the strong pump field spectrally separated from the produced pairs. However, the Raman side bands can be very broad. It is possible to imagine that despite the large spectral separation, the Stokes band will have some overlap with the nearest of the produced pairs, as we see in fig. 3.3. At the level of this Hamiltonian, the Raman effect can be pictured as a linear coupling to the ω_2 field,

$$\hat{H}_\text{I} = \hbar\Gamma \left(e^{i\Delta\phi} \hat{a}_1^\dagger \hat{a}_2^\dagger + e^{-i\Delta\phi} \hat{a}_1 \hat{a}_2\right) + \hbar\gamma' \left(\hat{a}_2^\dagger + \hat{a}_2\right), \tag{2.25}$$

where γ' is some effective nonlinearity.

As before, this Hamiltonian has no explicit time-dependence, so the solution to Schrödinger's equation is given by the time-evolution operator,

$$\begin{aligned} U_\text{I}(t) &= e^{-i\hat{H}_\text{I} t/\hbar} \\ &= \exp\left[-i\Gamma t \left(e^{i\Delta\phi} \hat{a}_1^\dagger \hat{a}_2^\dagger + e^{-i\Delta\phi} \hat{a}_1 \hat{a}_2\right) - i\gamma' t \left(\hat{a}_2^\dagger + \hat{a}_2\right)\right] \\ &= e^{\xi \hat{a}_1^\dagger \hat{a}_2^\dagger - \xi^* \hat{a}_1 \hat{a}_2 + \kappa \hat{a}_2^\dagger - \kappa^* \hat{a}_2} \end{aligned} \tag{2.26}$$

where $\xi = -i\Gamma e^{i\Delta\phi} t$ as before, and $\kappa = -i\gamma' t$. Expanding in small ξ and κ, this gives us the

following state:

$$\begin{aligned}
U_{\mathrm{I}}(t)\,|\mathrm{vac}\rangle \approx\; & |\mathrm{vac}\rangle + \xi \hat{a}_1^\dagger \hat{a}_2^\dagger\,|\mathrm{vac}\rangle \\
& - \frac{|\xi|^2}{2}\hat{a}_1\hat{a}_2\hat{a}_1^\dagger\hat{a}_2^\dagger\,|\mathrm{vac}\rangle + \frac{\xi^2}{2}\left(\hat{a}_1^\dagger\hat{a}_2^\dagger\right)^2|\mathrm{vac}\rangle \\
& - \frac{|\kappa|^2}{2}\hat{a}_2\hat{a}_2^\dagger\,|\mathrm{vac}\rangle + \kappa\xi\hat{a}_1^\dagger\hat{a}_2^\dagger\hat{a}_2^\dagger\,|\mathrm{vac}\rangle - \frac{\kappa^*\xi}{2}\hat{a}_2\hat{a}_1^\dagger\hat{a}_2^\dagger\,|\mathrm{vac}\rangle \\
& + \kappa\hat{a}_2^\dagger\,|\mathrm{vac}\rangle + \frac{\kappa^2}{2}\hat{a}_2^\dagger\hat{a}_2^\dagger\,|\mathrm{vac}\rangle + \ldots \\
=\; & \left(1 - \frac{|\xi|^2}{2} - \frac{|\kappa|^2}{2}\right)|\mathrm{vac}\rangle + \xi\,|1,1\rangle + \xi^2\,|2,2\rangle \\
& - \kappa\,|0,1\rangle + \frac{\kappa^2}{\sqrt{2}}\,|0,2\rangle + \sqrt{2}\kappa\xi\,|1,2\rangle - \frac{\kappa^*\xi}{2}\,|1,0\rangle + \ldots
\end{aligned} \tag{2.27}$$

Now, not only do we have the pairs from eq. (2.24), we also have unmatched photons from the Raman term in our Hamiltonian, such as $|0,1\rangle$ and $|1,0\rangle$. The $|0,1\rangle$ term comes from the Stokes process (i.e. the addition of a photon, $|0,0\rangle \to |0,1\rangle$). The $|1,0\rangle$ term comes from the anti-Stokes process (i.e. the removal of a photon from that mode, $|1,1\rangle \to |1,0\rangle$). If we are trying to herald the presence of a signal photon, the herald may in fact be a Raman photon – there will be no corresponding signal photon. For the anti-Stokes process, our signal photon is present, but it is no longer heralded.

Probably the last sound heard before the Universe folded up like a paper hat would be someone saying, 'What happens if I do this?'

Sir Terry Pratchett, *Interesting Times*

3 Formalism

We now proceed to develop the full Hamiltonian for SSTPDC. When generating single photons using nonlinear optical processes, due to the exceedingly small magnitude of the $\chi^{(3)}$ nonlinearity, we typically must use ultrashort pulses of high intensity light in waveguides designed for tight mode confinement, in order to produce useful quantities of photons. Such short pulse durations bring with them a host of nonlinear effects, including self and cross phase modulation, but also imply broad frequency spectra and the treatment must be multimode in nature, as we see in fig. 3.1. As such, the Hamiltonian must be in the fully multimode regime, accounting for the frequency profiles of the fields and the waveguides in which the fields are guided.

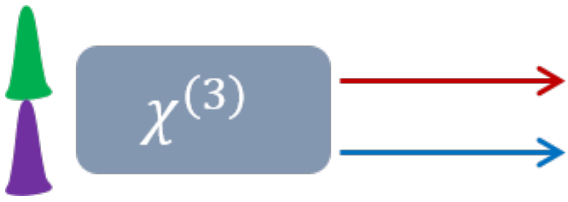

Figure 3.1

Figure 3.2: A diagram showing pulses entering a $\chi^{(3)}$ material and producing pairs of photons.

In this chapter, we will first find the general Schrödinger Hamiltonian for SSTPDC. As we wish to calculate rates in chapter 4, we find the Hamiltonian for a specific waveguide

problem and move to the interaction picture to remove the linear evolution. Finally we use this interaction Hamiltonian to construct the joint state intensity for SSTPDC by finding the first order solution to Schrödinger's equation.

3.1 The nonlinear optical Hamiltonian and Schrödinger's Equation

The classical energy density for the electromagnetic field in a dispersionless medium is given by

$$U_{\text{em}} = \frac{1}{2}\epsilon \left|\mathbf{E}(\mathbf{r},t)\right|^2 + \frac{1}{2\mu}\left|\mathbf{B}(\mathbf{r},t)\right|^2,$$

where $\mathbf{E}$ is the electric field, $\mathbf{B}$ is the magnetic field, ϵ is the electric permittivity and μ is the magnetic permeability. This is very general, and the physics of a particular process (*e.g.* self-phase modulation, cross-phase modulation, *etc.*) is determined by elaborating the nature of ϵ and μ. Motivated by this, it is typical to write down the following quantum Hamiltonian

$$\hat{H} = \int_V \mathrm{d}^3\mathbf{r}\left[\frac{1}{2}\epsilon\left|\hat{\mathbf{E}}(\mathbf{r},t)\right|^2 + \frac{1}{2\mu}\left|\hat{\mathbf{B}}(\mathbf{r},t)\right|^2\right].$$

However, the preference for the electric field $\mathbf{E}$ over the displacement field $\mathbf{D}$ is arbitrary. In fact, the following Hamiltonian in terms of $\mathbf{D}$ and $\mathbf{B}$ is often more useful when working with optical processes in media.

$$H = \frac{1}{2}\int_V \mathrm{d}^3\mathbf{r}\left[\frac{1}{\mu_0}\int B^i \mathrm{d}B^i + \frac{1}{\epsilon_0}\int \left(D^i - P^i\right)\mathrm{d}D^i\right], \tag{3.1}$$

where now $\mu \approx \mu_0$ (as per usual in optics). This is because $\mathbf{D}$ and $\mathbf{B}$ are automatically transverse in a medium (and so two of Maxwell's equations are satisfied), where we are now using the Einstein summation convention to express components of vectors,

The polarisation is now given by an expansion in $\mathbf{D}$, which we write as

$$P^i = \Gamma^{(1)}_{ij}D^j + \Gamma^{(2)}_{ijm}D^jD^m + \Gamma^{(3)}_{ijmn}D^jD^mD^n + \ldots.$$

This is an equivalent expansion to the familiar one ($P^i = \epsilon_0\chi^{(1)}_{ij}E^j + \epsilon_0\chi^{(2)}_{ijm}E^jE^m + \ldots$). This new series of tensors $\Gamma^{(i)}$ is related to the usual nonlinear susceptibility tensors $\chi^{(i)}$ (see

appendix A.1). So now our full nonlinear Hamiltonian is

$$\begin{aligned} H = &\frac{1}{2\mu_0}\int_V \mathrm{d}^3\mathbf{r}\, B^i B^i + \frac{1}{2\epsilon_0}\int_V \mathrm{d}^3\mathbf{r}\, D^i D^i \\ &- \frac{1}{2\epsilon_0}\int_V \mathrm{d}^3\mathbf{r}\, \Gamma^{(1)}_{ij} D^i D^j - \frac{1}{3\epsilon_0}\int_V \mathrm{d}^3\mathbf{r}\, \Gamma^{(2)}_{ijm} D^i D^j D^m \\ &- \frac{1}{4\epsilon_0}\int_V \mathrm{d}^3\mathbf{r}\, \Gamma^{(3)}_{ijmn} D^i D^j D^m D^n + \dots \end{aligned} \tag{3.2}$$

The nonlinear Hamiltonian described by eq. (3.2) is very general and can be used to describe any $\chi^{(n)}$ process we might wish to examine, including SPDC and SFWM. In fact, this strategy has been employed previously by Yang, Liscidini and Sipe in 2008 for SPDC in waveguides [40]. Our treatment of SSTPDC will be similar, but the physical process itself is different. As SSTPDC is a purely third order process, we need only examine the third order term in eq. (3.2) (the final line), which we will denote $\hat{H}_{\mathrm{NL}}$.

The final goal is to construct the joint spectral intensity of a pair of photons in the interaction picture. From there we can understanding the necessary phasematching, the rate at which we can produce pairs, the correlations between pairs, and the impact of noise. We will seek for a solution to the Schrödinger equation,

$$i\frac{\mathrm{d}}{\mathrm{d}t}\left|\psi(t)\right\rangle = \hat{H}_{\mathrm{I}}(t)\left|\psi(t)\right\rangle, \tag{3.3}$$

where $\hat{H}_{\mathrm{I}}(t) = \mathrm{e}^{i\hat{H}_{\mathrm{L}}t/\hbar}\hat{H}_{\mathrm{NL}}\mathrm{e}^{-i\hat{H}_{\mathrm{L}}t/\hbar}$ is the nonlinear term in an interaction picture, so that the linear dynamics of the waveguide given by the usual linear Hamiltonian $\hat{H}_{\mathrm{L}}$ (the first line in eq. (3.2)) have been removed. The formal solution to eq. (3.3) is

$$\left|\psi(t)\right\rangle = \exp\left(\mathcal{T}\left[-i\int_{-\infty}^{\infty}\mathrm{d}t\,\hat{H}_{\mathrm{I}}(t)\right]\right)\left|\psi_{\mathrm{in}}\right\rangle, \tag{3.4}$$

where $\mathcal{T}$ is the time-ordering operator. In general, time-ordering operations are very complex. Even using sophisticated expansions such as the Magnus series, it is rarely possible to calculate anything beyond the first few terms [41, 42]. However, for now we simply take the first order expansion of this solution so that time-ordering drops out (these higher order terms are very weak due to the small magnitude of $\chi^{(3)}$), and we have

$$\left|\psi(t)\right\rangle \approx \left[1 - \frac{i}{\hbar}\int_{-\infty}^{\infty}\mathrm{d}t\,\hat{H}_{\mathrm{I}}(t)\right]\left|\psi_{\mathrm{in}}\right\rangle. \tag{3.5}$$

As we are concerned with pair generation, we take $\left|\psi_{\mathrm{in}}\right\rangle = \left|\mathrm{vac}\right\rangle$. However, first we must extract from eq. (3.2) only the physics relevant to SSTPDC.

3.2 The SSTPDC Hamiltonian

Maintaining the use of the Einstein summation convention, the quantum third order term of our Hamiltonian is

$$\hat{H}_{\mathrm{NL}} = -\frac{1}{4\varepsilon_0}\int \mathrm{d}^3\mathbf{r}\,\Gamma_3^{ijmn}(\mathbf{r})\hat{D}^i(\mathbf{r})\hat{D}^j(\mathbf{r})\hat{D}^m(\mathbf{r})\hat{D}^n(\mathbf{r}), \tag{3.6}$$

where we integrate over all volume, and sum over all vector components of the displacement field D^i. We need to frame this expression in terms of a waveguide with some $\epsilon(x, y)$ and $\chi^{(3)}(x, y, z)$ profile. To that end, it is convenient to express the displacement field operators as a sum over modes

$$\hat{\mathbf{D}} = \sum_{\gamma}\int_0^{\infty}\mathrm{d}k\,\sqrt{\frac{\hbar\omega_k}{2}}\mathbf{D}_{\gamma,k}(\mathbf{r})\hat{c}_{\gamma,k} + \mathrm{h.c.}, \tag{3.7}$$

where $\hat{c}_k$ are our usual bosonic annihilation operators indexed by wavenumber k and mode γ, we consider only forward propagating waves, and h.c. denotes the Hermitian conjugate. Note that whilst $\hat{\mathbf{D}}$ is an operator, $\mathbf{D}_{\gamma,k}$ is simply a complex function, representing modal solutions of the linear wave equation. By integrating over all k, we include all allowed frequencies, and the sum over γ incorporates all allowed spatial modes. Inserting eq. (3.7) into eq. (3.6), our Hamiltonian expands considerably

$$\begin{aligned}
\hat{H}_{\mathrm{NL}} = &-\frac{1}{4\varepsilon_0}\int \mathrm{d}^3\mathbf{r}\,\Gamma_3^{ijmn}(\mathbf{r}) \\
&\times\left[\sum_{\gamma_1}\int_0^{\infty}\mathrm{d}k_1\,\sqrt{\frac{\hbar\omega_{k_1}}{2}}\left(D^i_{\gamma_1,k_1}(\mathbf{r})\hat{c}_{\gamma_1,k_1} + \left[D^i_{\gamma_1,k_1}(\mathbf{r})\right]^*\hat{c}^{\dagger}_{\gamma_1,k_1}\right)\right] \\
&\times\left[\sum_{\gamma_2}\int_0^{\infty}\mathrm{d}k_2\,\sqrt{\frac{\hbar\omega_{k_2}}{2}}\left(D^j_{\gamma_2,k_2}(\mathbf{r})\hat{c}_{\gamma_2,k_2} + \left[D^j_{\gamma_2,k_2}(\mathbf{r})\right]^*\hat{c}^{\dagger}_{\gamma_2,k_2}\right)\right] \\
&\times\left[\sum_{\gamma_3}\int_0^{\infty}\mathrm{d}k_3\,\sqrt{\frac{\hbar\omega_{k_3}}{2}}\left(D^m_{\gamma_3,k_3}(\mathbf{r})\hat{c}_{\gamma_3,k_3} + \left[D^m_{\gamma_3,k_3}(\mathbf{r})\right]^*\hat{c}^{\dagger}_{\gamma_3,k_3}\right)\right] \\
&\times\left[\sum_{\gamma_4}\int_0^{\infty}\mathrm{d}k_4\,\sqrt{\frac{\hbar\omega_{k_4}}{2}}\left(D^n_{\gamma_4,k_4}(\mathbf{r})\hat{c}_{\gamma_4,k_4} + \left[D^n_{\gamma_4,k_4}(\mathbf{r})\right]^*\hat{c}^{\dagger}_{\gamma_4,k_4}\right)\right].
\end{aligned} \tag{3.8}$$

Note we have integrals over k for each mode in the nonlinear product. Phasematching will help to eliminate some of them, but the main task of this chapter is to reduce this Hamiltonian to something manageable.

3.2.1 Phasematching and notation

Due to the large spectral separation between the pump and seed in SSTPDC, it would be exceptionally difficult to phasematch using only a single mode. Trying to quasi-phasematch using techniques like periodic poling is possible in $\chi^{(3)}$ materials, but it is much more difficult than it is for $\chi^{(2)}$ materials [43, 44]. However, we can exploit higher order modal dispersion by operating in different waveguide modes in the upper and lower frequency bands. Later we will consider two fibre modes, HE_{11} and HE_{21} (see chapter 4), in two distinct respective frequency ranges, $\omega_k < \omega_H$ and $\omega_k > \omega_H$, where $\omega_H = (\omega_s + \omega_p)/2$, with ω_s and ω_p being the seed and pump frequencies, respectively. Even if other modes are supported, they will almost certainly not be automatically phasematched. To make distinguishing between the pump and seed fields clearer in expressions like eq. (3.8), we introduce new operators $\hat{a}_k$ and $\hat{b}_k$ such that

$$\hat{a}_k = \begin{cases} 0 & \text{if } k > \omega_H/v_p, \\ \hat{c}_{k,\mathrm{HE}_{11}} & \text{if } k \leq \omega_H/v_p, \end{cases} \tag{3.9}$$

and

$$\hat{b}_k = \begin{cases} \hat{c}_{k,\mathrm{HE}_{21}} & \text{if } k > \omega_H/v_p, \\ 0 & \text{if } k \leq \omega_H/v_p. \end{cases} \tag{3.10}$$

Here ω_H is a frequency demarcating the high and low frequency regions, and v_p is the phase velocity at ω_H. Defined in this manner, $\hat{a}_k$ represents the low frequency HE_{11} modes and $\hat{b}_k$ represents the high frequency HE_{21} modes. We similarly identify displacement field mode functions

$$D_k^i(\mathbf{r}) = \begin{cases} 0 & \text{if } k > \omega_H/v_p, \\ D^i_{k,\mathrm{HE}_{11}}(\mathbf{r}) & \text{if } k \leq \omega_H/v_p, \end{cases} \tag{3.11}$$

and

$$F_k^i(\mathbf{r}) = \begin{cases} D^i_{k,\mathrm{HE}_{12}}(\mathbf{r}) & \text{if } k > \omega_H/v_p, \\ 0 & \text{if } k \leq \omega_H/v_p, \end{cases} \tag{3.12}$$

so that D_k^i corresponds to the non-pump fields and F_k^i corresponds to the pump field.

Making these substitutions helps to make the physical processes more visible amongst

the algebra. The Hamiltonian now looks like

$$\begin{aligned}\hat{H}_{\mathrm{NL}} = &-\frac{1}{4\varepsilon_0}\int \mathrm{d}^3\mathbf{r}\,\Gamma_3^{ijmn} \\ &\times\left[\int_0^\infty \mathrm{d}k_1 \sqrt{\frac{\hbar\omega_{k_1}}{2}}\left(D^i_{k_1}\hat{a}_{k_1} + F^i_{k_1}\hat{b}_{k_1} + \left(D^i_{k_1}\right)^*\hat{a}^\dagger_{k_1} + \left(F^i_{k_1}\right)^*\hat{b}^\dagger_{k_1}\right)\right] \\ &\times\left[\int_0^\infty \mathrm{d}k_2 \sqrt{\frac{\hbar\omega_{k_2}}{2}}\left(D^j_{k_2}\hat{a}_{k_2} + F^j_{k_2}\hat{b}_{k_2} + \left(D^j_{k_2}\right)^*\hat{a}^\dagger_{k_2} + \left(F^j_{k_2}\right)^*\hat{b}^\dagger_{k_2}\right)\right] \\ &\times\left[\int_0^\infty \mathrm{d}k_3 \sqrt{\frac{\hbar\omega_{k_3}}{2}}\left(D^m_{k_3}\hat{a}_{k_3} + F^m_{k_3}\hat{b}_{k_3} + \left(D^m_{k_3}\right)^*\hat{a}^\dagger_{k_3} + \left(F^m_{k_3}\right)^*\hat{b}^\dagger_{k_3}\right)\right] \\ &\times\left[\int_0^\infty \mathrm{d}k_4 \sqrt{\frac{\hbar\omega_{k_4}}{2}}\left(D^n_{k_4}\hat{a}_{k_4} + F^n_{k_4}\hat{b}_{k_4} + \left(D^n_{k_4}\right)^*\hat{a}^\dagger_{k_4} + \left(F^n_{k_4}\right)^*\hat{b}^\dagger_{k_4}\right)\right].\end{aligned} \tag{3.13}$$

In this form, we can see all possible combinations of fields. Now can we expand this and keep only the terms relevant to SSTPDC (*i.e.* only those involving a single pump field, F^i_k). For now we neglect the cross and self-phase modulation terms [45]. The most general form of the SSTPDC Hamiltonian is thus

$$\begin{aligned}\hat{H}_{\mathrm{SSTPDC}} = &-\frac{1}{4\varepsilon_0}\int \mathrm{d}^3\mathbf{r}\,\Gamma_3^{ijmn}\int_0^\infty \mathrm{d}k_1\int_0^\infty \mathrm{d}k_2\int_0^\infty \mathrm{d}k_3\int_0^\infty \mathrm{d}k_4\sqrt{\frac{\hbar^4\omega_{k_1}\omega_{k_2}\omega_{k_3}\omega_{k_4}}{2^4}} \\ &\times\Big[\left\{\left(D^i_{k_1}D^j_{k_2}D^m_{k_3}\right)^* F^n_{k_4} + \left(D^i_{k_1}D^j_{k_2}D^n_{k_3}\right)^* F^m_{k_4}\right. \\ &\left.+\left(D^i_{k_1}D^n_{k_2}D^m_{k_3}\right)^* F^j_{k_4} + \left(D^n_{k_1}D^j_{k_2}D^m_{k_3}\right)^* F^i_{k_4}\right\}\,\hat{a}^\dagger_{k_1}\hat{a}^\dagger_{k_2}\hat{a}^\dagger_{k_3}\hat{b}_{k_4} + \mathrm{h.c}\Big].\end{aligned} \tag{3.14}$$

Each of these terms looks like the annihilation of one photon ($\hat{b}_{k_4}$) and the creation of three photons ($\hat{a}^\dagger_{k_1}$, $\hat{a}^\dagger_{k_2}$, $\hat{a}^\dagger_{k_3}$), and vice versa. There are no terms describing the annihilation of two photons and the creation of two photons, as we would expect from SFWM.

3.2.2 Introducing waveguides

As we are interested primarily in waveguide geometries, we can write modes as the product of a transverse mode function and a longitudinal plane wave, or

$$\begin{aligned}\mathbf{D}_k(\mathbf{r}) &= \frac{\mathbf{d}_k(x,y)\mathrm{e}^{ikz}}{\sqrt{2\pi}}, \\ \mathbf{F}_k(\mathbf{r}) &= \frac{\mathbf{f}_k(x,y)\mathrm{e}^{ikz}}{\sqrt{2\pi}},\end{aligned} \tag{3.15}$$

where we have introduced the factor of $1/\sqrt{2\pi}$ for convenience, and $\mathbf{d}_k$, $\mathbf{f}_k$ are solutions to the waveguide wave equation, found analytically or numerically.

As the pump and probe are bright classical laser fields it is appropriate and helpful to replace their full operators $\hat{a}_k$ by their mean values α_k. In our case, these fields are short pulses with some temporal profile $A_{p,s}\phi_{p,s}(t)$, where we will choose the envelopes to be normalised: $\int_{-\infty}^{\infty}\mathrm{d}t\ |\phi(t)|^2 \equiv 1$. In wavevector space, these are represented by Fourier transformed spectral envelopes $\phi_{s,i}(k)$. So we make the replacements $\hat{a}_k \to \alpha\phi_s(k) + \hat{a}_k$ and $\hat{b}_k \to \beta\phi_p(k) + \hat{b}_k$. We keep only terms that look like $\phi_p(k_4)\phi_s^*(k_3)\hat{a}^\dagger_{k_2}\hat{a}^\dagger_{k_1}$, *i.e.* the down-conversion of the pump $\phi_p(k)$, stimulating the seed field $\phi_s(k)$ and the creation of photon pairs $\hat{a}^\dagger_{k_1}\hat{a}^\dagger_{k_2}$. Finally, we return to the familiar nonlinear susceptibility χ rather than Γ (using a result from appendix A.1), where

$$\Gamma^{(3)}_{ijmn} = \frac{\chi^{(3)}_{ijmn}}{\varepsilon_0^2 n_0^8}.$$

To include the effect of the material dispersion, we recognise that each field contributes a factor of n_0^2 to Γ_3, which we now associate with a frequency-dependent $n^2(x, y; \omega_k)$. We will abbreviate this to n_k^2. This gives us

$$\begin{aligned} H_{\text{SSTPDC}} = &-\frac{3\alpha^*\beta\hbar^2}{\pi^2\,(4\varepsilon_0)^3}\int \mathrm{d}^3\mathbf{r}\,\chi^{(3)}_{ijmn}\int_0^\infty \mathrm{d}k_1\int_0^\infty \mathrm{d}k_2\int_0^\infty \mathrm{d}k_3\int_0^\infty \mathrm{d}k_4\,\sqrt{\omega_{k_1}\omega_{k_2}\omega_{k_3}\omega_{k_4}} \\ &\times\left[\left(d^i_{k_1}d^j_{k_2}d^m_{k_3}\right)^* f^n_{k_4} + \left(d^i_{k_1}d^j_{k_2}d^n_{k_3}\right) f^m_{k_4} + \left(d^i_{k_1}d^n_{k_2}d^m_{k_3}\right) f^j_{k_4} + \left(d^n_{k_1}d^j_{k_2}d^m_{k_3}\right) f^i_{k_4}\right] \\ &\times\frac{\phi_s^*(k_3)\phi_p(k_4)\mathrm{e}^{i(k_4-k_3-k_2-k_1)z}}{n^2_{k_1}n^2_{k_2}n^2_{k_3}n^2_{k_4}}\hat{a}^\dagger_{k_1}\hat{a}^\dagger_{k_2} + \text{h.c.}. \end{aligned} \tag{3.16}$$

As there are three possible ways to combine the fields into the arrangement above, we acquire a factor of three.

Following Yang, Liscidini and Sipe (2008), we split the nonlinear susceptibility into two terms, a transverse profile and a longitudinal amplitude, $\chi^{(3)}(\mathbf{r}) = \chi^{(3)}(x, y)s(z)$, where we take $s(z) = 1$ for $-L/2 \le z \le L/2$. More general $s(z)$ can be considered later. We also define the following quantities

$$\mathfrak{s}(k) \equiv \int_{-\infty}^{\infty}\mathrm{d}z\,s(z)\mathrm{e}^{-ikz}, \tag{3.17}$$

$$\begin{aligned} \frac{1}{\mathcal{A}(k_1,k_2,k_3,k_4)} \equiv &\int_{-\infty}^{\infty}\mathrm{d}x\int_{-\infty}^{\infty}\mathrm{d}y\,\frac{\bar{n}^4\chi^{(3)}_{ijmn}(x,y)}{\overline{\chi}^{(3)}\varepsilon_0^2 n^2_{k_1}n^2_{k_2}n^2_{k_3}n^2_{k_4}} \\ &\times\left[\left(d^i_{k_1}d^j_{k_2}d^m_{k_3}\right)^* f^n_{k_4} + \left(d^i_{k_1}d^j_{k_2}d^n_{k_3}\right) f^m_{k_4} + \left(d^i_{k_1}d^n_{k_2}d^m_{k_3}\right) f^j_{k_4} + \left(d^n_{k_1}d^j_{k_2}d^m_{k_3}\right) f^i_{k_4}\right], \end{aligned} \tag{3.18}$$

(3.19)

where $\bar{n}$ is a typical value of the local refractive index and $\overline{\chi}^{(3)}$ is the typical size of one of the nonvanishing components of $\chi^{(3)}(x, y)$, introduced solely for convenience. It is also

convenient to have our fields normalised in such a way that their energy represents a single discrete excitation of energy $\hbar\omega$, and to account for material dispersion [46]. Thus, we normalise our fields according to

$$\int \mathrm{d}x\,\mathrm{d}y\,\frac{d_k(x,y)d_k^*(x,y)}{\varepsilon_0 n^2(x,y;\omega_k)} \equiv 1. \tag{3.20}$$

By examining eq. (3.20), we determine that d_k must have dimensions equal to $\sqrt{\varepsilon_0}/L$. This means that $\mathcal{A}$ has units of area, and similar to the classical case from section 2.1, we think of it as the effective coupling area between modes. After the manipulations in eqs. (3.17) to (3.20), we arrive at the final form of our Hamiltonian,

$$\hat{H}_{\mathrm{SSTPDC}} = -\frac{3\alpha\beta\hbar^2}{64\pi^2\epsilon_0}\int_0^\infty \mathrm{d}k_1 \int_0^\infty \mathrm{d}k_2 \int_0^\infty \mathrm{d}k_3 \int_0^\infty \mathrm{d}k_4\,\sqrt{\omega_{k_1}\omega_{k_2}\omega_{k_3}\omega_{k_4}} \frac{\mathfrak{s}^*(k_4-k_3-k_2-k_1)\overline{\chi}^{(3)}}{\bar{n}^4}\frac{\phi_s^*(k_3)\phi_p(k_4)}{\mathcal{A}(k_1,k_2,k_3,k_4)}\hat{a}_{k_1}^\dagger\hat{a}_{k_2}^\dagger + \mathrm{h.c.} \tag{3.21}$$

All of the SSTPDC physics is contained in this expression, eq. (3.21). The rest of the work of this chapter is to extract the physics in a meaningful way.

3.2.3 Comparison with SPDC and SFWM

This Hamiltonian is quite similar to both the familiar SPDC and SFWM Hamiltonians, which are respectively [26]

$$\begin{aligned}\hat{H}_{\mathrm{SPDC}} &= -\int_0^\infty \mathrm{d}k_1 \int_0^\infty \mathrm{d}k_2 \int_0^\infty \mathrm{d}k\, S_{\mathrm{SPDC}}(k,k_1,k_2)\hat{a}_{k_1}^\dagger\hat{a}_{k_2}^\dagger + \mathrm{h.c.},\\ \hat{H}_{\mathrm{SFWM}} &= -\int_0^\infty \mathrm{d}k_1 \int_0^\infty \mathrm{d}k_2 \int_0^\infty \mathrm{d}k_3 \int_0^\infty \mathrm{d}k_4\, S_{\mathrm{SFWM}}(k_1,k_2,k_3,k_4)\hat{a}_{k_1}^\dagger\hat{a}_{k_2}^\dagger,\end{aligned} \tag{3.22}$$

where $S(k)$ accounts for the specific fields and nonlinearities involved [26].

SPDC is a three-wave mixing interaction that annihilates a pump photon to create a pair of photons, SFWM is a four-wave mixing interaction that annihilates two pump photons to create a pair of photons, and SSTPDC is a four-wave mixing interaction that annihilates a pump photon to create a triplet of photons, though seeded by an additional field so as to create a pair of accessible photons. We also note that from eq. (3.14) we could have kept terms that involve the creation of two photons at the centre frequency of the seed, leaving just a *single* accessible photon, and arrived at

$$\hat{H}_{\mathrm{SSDTPDC}} = -\int_0^\infty \mathrm{d}k_1 \int_0^\infty \mathrm{d}k_2 \int_0^\infty \mathrm{d}k_3 \int_0^\infty \mathrm{d}k_4\, S_{\mathrm{SDSTPDC}}(k_1,k_2,k_3,k_4)\hat{a}_{k_1}^\dagger + \mathrm{h.c.}, \tag{3.23}$$

where

$$S_{\text{SSDTPDC}}(k_1,k_2,k_3,k_4) \equiv \frac{3\,(\alpha^*)^2\,\beta\hbar^2}{64\pi^2\varepsilon_0}\sqrt{\omega_{k_1}\omega_{k_2}\omega_{k_3}\omega_{k_4}}\frac{\mathfrak{s}^*(k_4-k_3-k_2-k_1)\overline{\chi}^{(3)}}{\bar{n}^4} \times \frac{\phi_s^*(k_2)\phi_s^*(k_3)\phi_p(k_4)\mathrm{e}^{i(\omega_{k_2}+\omega_{k_3}-\omega_{k_4})t}}{\mathcal{A}(k_1,k_2,k_3,k_4)}.$$

However, as a first approximation, we imagine that these terms can be ignored on the grounds that they are not as well phase matched as the main process is. Also, if the pump is at the third harmonic and the seed is truly at the fundamental frequency, conservation of energy does not allow this process to occur.

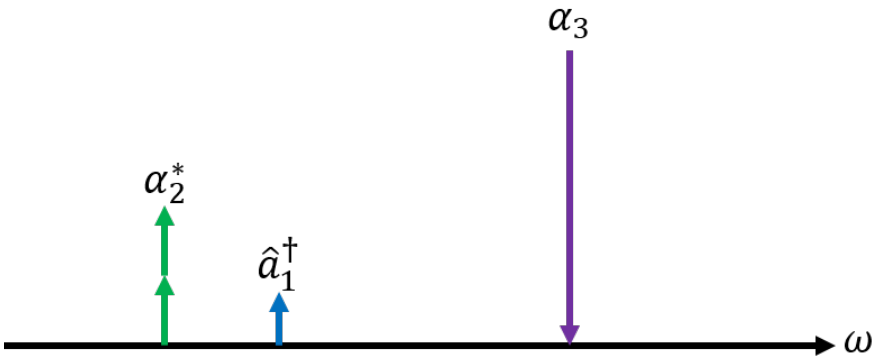

Figure 3.3: A process similar to SSTPDC that generates a single accessible photon.

3.3 The Interaction Hamiltonian

We now have found the Schrödinger Hamiltonian specific to SSTPDC. Now we move into the interaction picture, to avoid explicitly dealing with the linear evolution, to find a solution to eq. (3.4). Using the form of the linear Hamiltonian shown in appendix A.2,

$$\hat{H}_{\text{L}} = \int_0^\infty \mathrm{d}k\,\hbar\left[\omega_k^{(\text{HE}_{11})}\hat{a}_k^\dagger\hat{a}_k + \omega_k^{(\text{HE}_{21})}\hat{b}_k^\dagger\hat{b}_k\right],$$

we transform the Schrödinger Hamiltonian to find

$$\hat{H}_{\text{I}}(t) = \exp\left(i\int_0^\infty \mathrm{d}k\,\left[\omega_k^{(\text{HE}_{11})}\hat{a}_k^\dagger\hat{a}_k + \omega_k^{(\text{HE}_{21})}\hat{b}_k^\dagger\hat{b}_k\right]t\right)\cdot\hat{H}_{\text{SSTPDC}} \cdot\exp\left(-i\int_0^\infty \mathrm{d}k\,\left[\omega_k^{(\text{HE}_{11})}\hat{a}_k^\dagger\hat{a}_k + \omega_k^{(\text{HE}_{21})}\hat{b}_k^\dagger\hat{b}_k\right]t\right). \quad (3.24)$$

Carrying around the mode indices on these ω_k terms is cumbersome, so we neglect to write them from here on and simply recall that $\omega_k^{(\text{HE}_{11})}$ is associated with $\hat{a}_k^\dagger\hat{a}_k$ and $\omega_k^{(\text{HE}_{21})}$ is associated with $\hat{b}_k^\dagger\hat{b}_k$. Now the creation operators $\hat{a}_{k_1}^\dagger$ and $\hat{a}_{k_2}^\dagger$ are tangled in between

exponentials that they do not necessarily commute with. To disentangle them, we use the results

$$e^{\chi \hat{I}} \hat{c}_{k_1}^\dagger e^{-\chi \hat{I}} = \hat{c}_{k_1}^\dagger e^{\omega_{k_1} \chi}, \tag{3.25}$$

$$e^{\chi \hat{I}} \hat{c}_{k_1} e^{-\chi \hat{I}} = \hat{c}_{k_1} e^{-\omega_{k_1} \chi}, \tag{3.26}$$

as derived in appendix A.3, where $\chi = it$, $\hat{I} = \int_0^\infty \mathrm{d}k\, \omega_k \hat{c}_k^\dagger \hat{c}_k$.

Recognising that $\exp\left(i \int_0^\infty \mathrm{d}k\, \omega_k \hat{a}_k^\dagger \hat{a}_k t\right)$ will commute with $\exp\left(i \int_0^\infty \mathrm{d}k\, \omega_k \hat{b}_k^\dagger \hat{b}_k t\right)$ due to the distinct frequency intervals they cover as defined by eqs. (3.9) and (3.10), eq. (3.24) becomes an expression that looks very much like eq. (3.25). Inserting $\exp\left(i \int_0^\infty \mathrm{d}k\, \hat{a}_k^\dagger \hat{a}_k t\right) \cdot \exp\left(-i \int_0^\infty \mathrm{d}k\, \hat{a}_k^\dagger \hat{a}_k t\right) = 1$ between $\hat{a}_{k_1}^\dagger$ and $\hat{a}_{k_2}^\dagger$ allows us to apply this identity twice, yielding

$$\begin{aligned}\hat{H}_1(t) = &-\frac{3\alpha\beta\hbar^2}{64\pi^2\epsilon_0} \int_0^\infty \mathrm{d}k_1 \int_0^\infty \mathrm{d}k_2 \int_0^\infty \mathrm{d}k_3 \int_0^\infty \mathrm{d}k_4\, \sqrt{\omega_{k_1}\omega_{k_2}\omega_{k_3}\omega_{k_4}} \frac{\mathfrak{s}^*(k_4 - k_3 - k_2 - k_1)\overline{\chi}^{(3)}}{\bar{n}^4} \\ &\times \frac{\phi_s^*(k_3)\phi_p(k_4) e^{-i(\omega_{k_4} - \omega_{k_3} - \omega_{k_2} - \omega_{k_1})t}}{\mathcal{A}(k_1, k_2, k_3, k_4)} \hat{a}_{k_1}^\dagger \hat{a}_{k_2}^\dagger + \text{h.c.}\end{aligned} \tag{3.27}$$

The oscillating exponential term, $e^{-i(\omega_{k_4} - \omega_{k_3} - \omega_{k_2} - \omega_{k_1})t}$, will become exceptionally useful in section 3.4. We note that the factor of $e^{-i(\omega_{k_4} - \omega_{k_3})t}$ has been included here also. If the classical fields had been introduced after using the identities eq. (3.25), this factor would have appeared naturally.

3.4 The first order solution

Having found the interaction Hamiltonian, we can at last find the first order solution, eq. (3.5). Upon integrating eq. (3.27) with respect to all time (as the interaction Hamiltonian will be zero outside of the medium [47]), the oscillating exponential term acts as a representation of the Dirac delta function, $2\pi\delta\left(\omega_{k_4} - \omega_{k_3} - \omega_{k_2} - \omega_{k_1}\right)$. So the solution takes the form

$$\begin{aligned}|\psi_{\text{out}}\rangle \approx |\text{vac}\rangle + \frac{3i\alpha^*\beta\hbar}{32\pi\varepsilon_0} &\int_0^\infty \mathrm{d}k_1 \int_0^\infty \mathrm{d}k_2 \int_0^\infty \mathrm{d}k_3 \int_0^\infty \mathrm{d}k_4\, \delta(\omega_{k_4} - \omega_{k_3} - \omega_{k_2} - \omega_{k_1}) \\ &\times \sqrt{\omega_{k_1}\omega_{k_2}\omega_{k_3}\omega_{k_4}} \frac{\mathfrak{s}^*(k_4 - k_3 - k_2 - k_1)\bar{\chi}_3}{\bar{n}^4} \frac{\phi_s^*(k_3)\phi_p(k_4)}{\mathcal{A}(k_1, k_2, k_3, k_4)} \hat{a}_{k_1}^\dagger \hat{a}_{k_2}^\dagger |\text{vac}\rangle\,.\end{aligned} \tag{3.28}$$

With a Dirac delta function sitting there waiting to be used, we are motivated to transform our integrals over k_i to ω_i. This transformation introduces the group velocity through $\frac{\mathrm{d}\omega_i}{\mathrm{d}k_i} = v_g(\omega_i)$. It is also important to maintain the appropriate dimensionality and the

canonical form of the commutator, $\left[\hat{a}_k, \hat{a}^\dagger_{k'}\right] = \delta\left(k - k'\right)$. To do so, we define new operators

$$\hat{a}_{\omega_i} \equiv \sqrt{\frac{\mathrm{d}k_i(\omega_i)}{\mathrm{d}\omega_i}}\hat{a}_{k_i}, \tag{3.29}$$

$$\hat{b}_{\omega_i} \equiv \sqrt{\frac{\mathrm{d}k_i(\omega_i)}{\mathrm{d}\omega_i}}\hat{b}_{k_i}. \tag{3.30}$$

With these definitions, one can show that they satisfy the natural commutators

$$\left[\hat{a}_{\omega_i}, \hat{a}^\dagger_{\omega_i'}\right] = \delta\left(\omega_i - \omega_i'\right),$$
$$\left[\hat{b}_{\omega_i}, \hat{b}^\dagger_{\omega_i'}\right] = \delta\left(\omega_i - \omega_i'\right).$$

To ensure that everything is correctly normalised later, in shifting to frequency pulse envelopes we also include a conversion factor

$$\bar{\phi}_s(\omega_i) = \sqrt{\frac{\mathrm{d}k_i(\omega_i)}{\mathrm{d}\omega_i}}\phi_s(k_i(\omega_i)),$$
$$\bar{\phi}_p(\omega_i) = \sqrt{\frac{\mathrm{d}k_i(\omega_i)}{\mathrm{d}\omega_i}}\phi_p(k_i(\omega_i)),$$

so now

$$\begin{aligned}|\psi_{\mathrm{out}}\rangle \approx |\mathrm{vac}\rangle + \frac{3i\alpha\beta\hbar}{32\pi\varepsilon_0}\int_0^\infty \mathrm{d}\omega_1 \int_0^\infty \mathrm{d}\omega_2 \int_0^\infty \mathrm{d}\omega_3 \int_0^\infty \mathrm{d}\omega_4\, \delta(\omega_4 - \omega_3 - \omega_2 - \omega_1)\\ \times \sqrt{\frac{\omega_1\,\omega_2\,\omega_3\,(\omega_1+\omega_2+\omega_3)}{v_g(\omega_1)v_g(\omega_2)v_g(\omega_3)v_g(\omega_1+\omega_2+\omega_3)}}\frac{\mathfrak{s}^*\left[k_p(\omega_4) - k_s(\omega_3) - k_s(\omega_2) - k_s(\omega_1)\right]\bar{\chi}_3}{\bar{n}^4}\\ \times \frac{\bar{\phi}_s^*(\omega_3)\bar{\phi}_p(\omega_4)}{\mathcal{A}\left[k(\omega_1), k(\omega_2), k(\omega_3), k(\omega_4)\right]}\hat{a}^\dagger_{\omega_1}\hat{a}^\dagger_{\omega_2}|\mathrm{vac}\rangle\,.\end{aligned} \tag{3.31}$$

Integrating with respect to $\mathrm{d}\omega_4$ and using the Dirac delta function then yields

$$\begin{aligned}|\psi_{\mathrm{out}}\rangle \approx |\mathrm{vac}\rangle + \frac{3i\alpha\beta\hbar}{32\pi\varepsilon_0}\int_0^\infty \mathrm{d}\omega_1 \int_0^\infty \mathrm{d}\omega_2 \int_0^\infty \mathrm{d}\omega \sqrt{\frac{\omega_1\,\omega_2\,\omega\,(\omega_1+\omega_2+\omega)}{v_g(\omega_1)v_g(\omega_2)v_g(\omega)v_g(\omega_1+\omega_2+\omega)}}\\ \times \frac{\mathfrak{s}^*(\Delta k)\,\bar{\chi}_3}{\bar{n}^4}\frac{\bar{\phi}_s^*(\omega)\bar{\phi}_p(\omega_1+\omega_2+\omega)}{\mathcal{A}\left[k(\omega_1), k(\omega_2), k(\omega), k(\omega_1+\omega_2+\omega)\right]}\hat{a}^\dagger_{\omega_1}\hat{a}^\dagger_{\omega_2}|\mathrm{vac}\rangle\,.\end{aligned} \tag{3.32}$$

where we have defined

$$\Delta k = k_p(\omega_1+\omega_2+\omega) - k_s(\omega) - k_s(\omega_2) - k_s(\omega_1), \tag{3.33}$$

with the subscripts denoting whether the wavenumber is associated with the pump field or

the low frequency seed field.

Similarly to eq. (2.24), we are looking for a single pair state. As we have taken only the first order approximation, higher order pairs do not appear here. We are looking for something of the form

$$\begin{aligned}|\psi_{\text{out}}\rangle &\approx \frac{1}{\sqrt{1+|\eta|^2}}\left[|\text{vac}\rangle + \frac{\eta}{\sqrt{2}}\int_0^\infty \mathrm{d}\omega_1 \int_0^\infty \mathrm{d}\omega_2\, \Phi(\omega_1,\omega_2)\hat{a}^\dagger_{\omega_1}\hat{a}^\dagger_{\omega_2}|\text{vac}\rangle\right] \\ &= \frac{|\text{vac}\rangle + \eta\,|\text{II}\rangle}{\sqrt{1+|\eta|^2}},\end{aligned} \tag{3.34}$$

where $|\text{II}\rangle$ is the two photon state (analogous to $|1,1\rangle$), and we define η in a moment. By comparison with eq. (3.32) we can identify the joint spectral amplitude $\phi(\omega_1,\omega_2)$ as

$$\begin{aligned}\Phi(\omega_1,\omega_2) =& \frac{3\sqrt{2}i\alpha\beta\hbar}{32\pi\varepsilon_0\eta}\int_0^\infty \mathrm{d}\omega \sqrt{\frac{\omega_1\,\omega_2\,\omega\,(\omega_1+\omega_2+\omega)}{v_g(\omega_1)v_g(\omega_2)v_g(\omega)v_g(\omega_1+\omega_2+\omega)}} \\ &\times \frac{\mathfrak{s}^*(\Delta k)\,\bar{\chi}_3}{\bar{n}^4}\frac{\bar{\phi}^*_s(\omega)\bar{\phi}_p(\omega_1+\omega_2+\omega)}{\mathcal{A}\left[k(\omega_1),k(\omega_2),k(\omega),k(\omega_1+\omega_2+\omega)\right]}.\end{aligned} \tag{3.35}$$

This is a full description of the biphoton state, as $\phi(\omega_1,\omega_2)$ is the JSA containing all information about the correlations, as well as the rate at which we can produce pairs.

If we choose the biphoton state to be normalised (*i.e.* $\langle\text{II}|\text{II}\rangle = 1$), then we can associate $|\eta|^2$ with the average probability of producing the state $|\text{II}\rangle$. That is to say, $|\eta|^2$ is the average probability of producing a single pair of photons per pump pulse. Explicitly we write

$$\langle\text{II}|\text{II}\rangle = \frac{1}{2}\int_0^\infty \mathrm{d}\omega_1' \int_0^\infty \mathrm{d}\omega_2' \int_0^\infty \mathrm{d}\omega_1 \int_0^\infty \mathrm{d}\omega_2\, \Phi^*(\omega_1',\omega_2')\Phi(\omega_1,\omega_2)\,\langle\text{vac}|\,\hat{a}_{\omega_1'}\hat{a}_{\omega_2'}\hat{a}^\dagger_{\omega_1}\hat{a}^\dagger_{\omega_2}|\text{vac}\rangle, \tag{3.36}$$

and, noting that by a sequence of normal orderings

$$\begin{aligned}\hat{a}_{\omega_1'}\hat{a}_{\omega_2'}\hat{a}^\dagger_{\omega_1}\hat{a}^\dagger_{\omega_2} =\ & \hat{a}^\dagger_{\omega_1}\hat{a}^\dagger_{\omega_2}\hat{a}_{\omega_1'}\hat{a}_{\omega_2'} + \hat{a}^\dagger_{\omega_1}\hat{a}_{\omega_2'}\delta(\omega_1'-\omega_2) + \hat{a}^\dagger_{\omega_1}\hat{a}_{\omega_1'}\delta(\omega_2'-\omega_2) + \hat{a}^\dagger_{\omega_2}\hat{a}_{\omega_2'}\delta(\omega_1'-\omega_1) \\ &+ \hat{a}^\dagger_{\omega_2}\hat{a}_{\omega_1'}\delta(\omega_1'-\omega_1) + \delta(\omega_2'-\omega_2)\delta(\omega_1'-\omega_1) + \delta(\omega_1'-\omega_2)\delta(\omega_2'-\omega_1)\end{aligned}$$

we can reduce this to

$$\langle\text{II}|\text{II}\rangle = \frac{1}{2}\int_0^\infty \mathrm{d}\omega_1 \int_0^\infty \mathrm{d}\omega_2\, \left(|\Phi(\omega_1,\omega_2)|^2 + \Phi^*(\omega_2,\omega_1)\Phi(\omega_1,\omega_2)\right). \tag{3.37}$$

For a single polarisation, the joint state intensity is symmetric under a permutation of indices (*i.e.* $\Phi(\omega_2,\omega_1) = \Phi(\omega_1,\omega_2)$), and so the insistence on the state being normalised also implies

a condition on the normalisation of the joint state intensity, namely

$$\langle \mathrm{II}|\mathrm{II}\rangle = \int_0^\infty \mathrm{d}\omega_1 \int_0^\infty \mathrm{d}\omega_2 \; |\Phi(\omega_1,\omega_2)|^2 = 1. \tag{3.38}$$

Thus applying this to eq. (3.35), the average probability of producing the pair state is

$$\begin{aligned} |\eta|^2 =& \frac{9\,|\alpha|^2\,|\beta|^2\,\hbar^2}{128\pi^2\varepsilon_0^2} \int_0^\infty \mathrm{d}\omega_1 \int_0^\infty \mathrm{d}\omega_2 \\ &\times \left| \int_0^\infty \mathrm{d}\omega \sqrt{\frac{\omega_1\omega_2\omega(\omega_1+\omega_2+\omega)}{v_g(\omega_1)v_g(\omega_2)v_g(\omega)v_g(\omega_1+\omega_2+\omega)}} \frac{\mathfrak{s}^*\,(\Delta k)\,\overline{\chi}^{(3)}}{\bar{n}^4} \right. \\ &\left. \times \frac{\bar{\phi}_s^*(\omega)\bar{\phi}_p(\omega_1+\omega_2+\omega)}{\mathcal{A}\,[k(\omega_1),k(\omega_2),k(\omega),k(\omega_1+\omega_2+\omega)]} \right|^2 . \end{aligned} \tag{3.39}$$

This equation, eq. (3.39), describes the rate of production of photon pairs. We will evaluate this rate in chapter 4.

3.5 Optical powers

We can proceed no further analytically without making some simplifying assumptions. However, to get eq. (3.39) to a form to which we can attribute physical meaning, we first need to associate the amplitudes $\bar{\phi}_i$ with optical powers. It is simple enough to see that the energy contained in a single pulse will be given by $E_I = N\hbar\omega_c \int \mathrm{d}\omega \left|\bar{\phi}_i(\omega)\right|^2$, where ω_c is the central frequency of the pulse, and N is the number of photons contained in the pulse ($|\alpha|^2$ for the pump field, and $|\beta|^2$ for the seed field). Then, the instantaneous power is $P_I = \left|\tilde{\phi}_i(t)\right|^2 E_I$, where

$$\left|\tilde{\phi}_i(t)\right|^2 = \left| \int \frac{\mathrm{d}\omega}{\sqrt{2\pi}} \bar{\phi}(\omega) \mathrm{e}^{i\omega t} \right|^2 . \tag{3.40}$$

As we do not have superfast detectors, a quantity we are more likely to measure is the average power, $P_{\mathrm{av}} = E_I R = R P_{\mathrm{pulse}}/\tau$, where P_{pulse} is often referred to as the "peak power", where R is the repetition rate of the laser and τ the pulse duration. Note that as we will primarily be dealing with Gaussian pulses, we are defining the pulse duration to be the full width at half maximum, $\tau = 2\sqrt{2\ln 2}\sigma$, where the standard deviation is given by $\sigma = \sqrt{\langle t^2\rangle - \langle t\rangle^2}$. Our first simplifying assumption is that our fields are Gaussian with a known pulse duration

$$\tilde{\phi}_i(t) = \frac{1}{\pi^{1/4}\sqrt{\tau_i}} \mathrm{e}^{-\left(\frac{t^2}{2\tau_i^2} + i\omega_i t\right)}.$$

Then, according to eq. (3.40), the Fourier transform must be

$$\bar{\phi}_i(\omega) = \frac{\sqrt{\tau_i}}{\pi^{1/4}} \mathrm{e}^{-\frac{1}{2}\tau_i^2(\omega-\omega_i)^2}. \tag{3.41}$$

3.6 Finding the rate of pair production

Now that we have established the model for our laser fields, we can continue to calculate the rate of pair production. Recognising that if $s(z) = 1$ for $-L/2 \leq z \leq L/2$, then $\mathfrak{s}^*(\Delta k) = L\,\mathrm{sinc}\left(\frac{\Delta k(\omega_1,\omega_2,\omega_3,\omega_4)L}{2}\right)$. This gives us

$$\begin{aligned}|\eta|^2 =& \frac{9\left(\overline{\chi}^{(3)}\right)^2 |\alpha|^2 |\beta|^2 \tau_s\tau_p\hbar^2 L^2}{128\pi^3\varepsilon_0^2\bar{n}^8} \int_0^\infty \mathrm{d}\omega_1 \int_0^\infty \mathrm{d}\omega_2 \\ &\times \left| \int_0^\infty \mathrm{d}\omega \sqrt{\frac{\omega_1\omega_2\omega(\omega_1+\omega_2+\omega)}{v_g(\omega_1)v_g(\omega_2)v_g(\omega)v_g(\omega_1+\omega_2+\omega)}} \frac{\mathrm{e}^{-\frac{1}{2}\tau_s^2(\omega-\omega_s)^2}\mathrm{e}^{-\frac{1}{2}\tau_p^2\left(\omega_1+\omega_2+\omega-\omega_p\right)^2}\,\mathrm{sinc}\left(\frac{\Delta kL}{2}\right)}{\mathcal{A}\left[k(\omega_1),k(\omega_2),k(\omega),k(\omega_1+\omega_2+\omega)\right]} \right|^2.\end{aligned} \tag{3.42}$$

This is still intractable. With the expectation that our seed laser will be quasi-continuous wave, or at least have considerably longer pulses than the pump (*i.e.* $\tau_s \gg \tau_p$), we can approximate this as

$$\begin{aligned}|\eta|^2 \approx& \frac{9\left(\overline{\chi}^{(3)}\right)^2 |\alpha|^2 |\beta|^2 \tau_s\tau_p\hbar^2 L^2}{128\pi^3\varepsilon_0^2\bar{n}^8} \int_0^\infty \mathrm{d}\omega_1 \int_0^\infty \mathrm{d}\omega_2 \frac{\omega_1\omega_2\omega_s(\omega_1+\omega_2+\omega_s)}{v_g(\omega_1)v_g(\omega_2)v_g(\omega_s)v_g(\omega_1+\omega_2+\omega_s)} \\ &\times \frac{\mathrm{sinc}^2\left(\frac{\Delta kL}{2}\right)}{\mathcal{A}^2\left[k(\omega_1),k(\omega_2),k(\omega_s),k(\omega_1+\omega_2+\omega_s)\right]} \left| \int_0^\infty \mathrm{d}\omega\, \mathrm{e}^{-\frac{1}{2}\tau_s^2(\omega-\omega_s)^2}\mathrm{e}^{-\frac{1}{2}\tau_p^2\left(\omega_1+\omega_2+\omega-\omega_p\right)^2} \right|^2,\end{aligned}$$

as the Gaussians will vary much faster than the other quantities in the $\mathrm{d}\omega$ integrand.

Performing the innermost integration and expanding, we find

$$\begin{aligned}|\eta|^2 \approx& \frac{9\left(\overline{\chi}^{(3)}\right)^2 |\alpha|^2 |\beta|^2 \tau_s\tau_p\hbar^2 L^2}{128\pi^3\varepsilon_0^2\bar{n}^8} \int_0^\infty \mathrm{d}\omega_1 \int_0^\infty \mathrm{d}\omega_2 \frac{\omega_1\omega_2\omega_s(\omega_1+\omega_2+\omega_s)}{v_g(\omega_1)v_g(\omega_2)v_g(\omega_s)v_g(\omega_1+\omega_2+\omega_s)} \\ &\times \frac{\mathrm{sinc}^2\left(\frac{\Delta kL}{2}\right)}{\mathcal{A}^2\left[k(\omega_1),k(\omega_2),k(\omega_s),k(\omega_1+\omega_2+\omega_s)\right]} \frac{2\pi}{\tau_p^2+\tau_s^2} \mathrm{e}^{-\frac{\tau_p^2\tau_s^2}{\tau_p^2+\tau_s^2}\left(\omega_1+\omega_2+\omega_s-\omega_p\right)^2}.\end{aligned} \tag{3.43}$$

Recalling eq. (3.33), we now expand the wavenumber around the respective central frequency $\omega_c = \omega_{s,p}$;

$$\begin{aligned} k(\omega) &\approx k(\omega_c) + \left.\frac{\mathrm{d}k}{\mathrm{d}\omega}\right|_{\omega=\omega_c} (\omega - \omega_c) + \frac{1}{2} \left.\frac{\mathrm{d}^2 k}{\mathrm{d}\omega^2}\right|_{\omega=\omega_c} (\omega - \omega_c)^2 \\ &= k(\omega_c) + \frac{1}{v_g(\omega_c)} (\omega - \omega_c) + \frac{1}{2}\beta_2(\omega_c) (\omega - \omega_c)^2 . \end{aligned} \tag{3.44}$$

We can use this result to express Δk in the following manner;

$$\begin{aligned} \Delta k =& k(\omega_p) - 3k(\omega_s) + \frac{\omega_1 + \omega_2 + \omega_s - \omega_p}{v_g(\omega_p)} - \frac{\omega_1 + \omega_2 - 2\omega_s}{v_g(\omega_s)} \\ &+ \frac{1}{2}\beta_2(\omega_p) \left[\omega_1^2 + \omega_2^2 + \omega_s^2 + \omega_p^2 + 2\omega_1\omega_2 + 2\omega_1\omega_s - 2\omega_1\omega_p + 2\omega_2\omega_s - 2\omega_2\omega_p - 2\omega_s\omega_p\right] \\ &- \frac{1}{2}\beta_2(\omega_s) \left[\omega_1^2 + \omega_2^2 + 2\omega_s^2 - 2\omega_1\omega_s - 2\omega_2\omega_s\right] . \end{aligned}$$

Assuming that this process is phase matched to first order, $k(\omega_p) - 3k(\omega_s) = 0$, and operating with centre frequencies such that $\omega_p = 3\omega_s$, we are left with

$$\begin{aligned} \Delta k = (\omega_1 + \omega_2 - 2\omega_s) &\left(\frac{1}{v_g(\omega_p)} - \frac{1}{v_g(\omega_s)}\right) \\ &+ (\omega_1 + \omega_2 - 2\omega_s)^2 \left(\frac{1}{2}\beta_2(\omega_p) - \frac{1}{2}\beta_2(\omega_s)\right) \\ &- \beta_2(\omega_s) \left[\omega_1\omega_s + \omega_2\omega_s - \omega_1\omega_2 - \omega_s^2\right] . \end{aligned} \tag{3.45}$$

Furthermore, we approximate group velocities, the frequency terms sitting outside of the Gaussian and sinc functions, and effective areas as constant over the frequency ranges of interest and introduce the nonlinear parameter

$$\gamma = \frac{3\overline{\chi}^{(3)}\omega_p}{8\varepsilon_0 v_g(\omega_s)^{3/2} v_g(\omega_p)^{1/2} \bar{n}^4 \mathcal{A}},$$

to find

$$|\eta|^2 = \frac{|\alpha|^2 |\beta|^2 \tau_s \tau_p \gamma^2 \hbar^2 \omega_s^2 L^2}{\pi^2 \left(\tau_p^2 + \tau_s^2\right)} \int_0^\infty \mathrm{d}\omega_1 \int_0^\infty \mathrm{d}\omega_2 \, \mathrm{e}^{-\frac{\tau_p^2 \tau_s^2}{\tau_p^2 + \tau_s^2}(\omega_1 + \omega_2 - 2\omega_s)^2} \operatorname{sinc}^2\left(\frac{\Delta k L}{2}\right). \tag{3.46}$$

It is more natural to work with powers, so we introduce

$$P_s = \frac{\hbar\omega |\alpha|^2}{\tau_s}, \tag{3.47}$$

and

$$P_p = \frac{\hbar\omega\,|\beta|^2}{\tau_p}, \tag{3.48}$$

where these powers are nominal average *pulse* powers (related to the average power by $\bar{P} = P_j\sigma$, where σ is the duty cycle). Now we can express the rate of pair production as

$$|\eta|^2 = \frac{\gamma^2\tau_p^2\tau_s^2\omega_s P_p P_s L^2}{\pi^2\omega_p\left(\tau_p^2+\tau_s^2\right)}\int_0^\infty \mathrm{d}\omega_1\int_0^\infty \mathrm{d}\omega_2\,\mathrm{e}^{-\frac{\tau_p^2\tau_s^2}{\tau_p^2+\tau_s^2}(\omega_1+\omega_2-2\omega_s)^2}\,\mathrm{sinc}^2\left(\frac{\Delta kL}{2}\right), \tag{3.49}$$

making it clear that the rate is proportional to the square of the total power. However, as we desire $P_s \ll P_p$, the rate will only scale linearly with pump power.

Here the integrand is of order unity, so the integral is simply an area in $\left(\mathrm{s}^{-1}\right)^2$, $A_\omega \approx \Delta\omega_1\Delta\omega_2$. We note that the sinc that appears here has precisely the same form as the sinc that appeared in eq. (2.20), although we have no contribution from self or cross-phase modulation here. In the next chapter, we produce a set of parameters in order to find rates from eq. (3.49).

As with most of life's problems,
this one can be solved by a box
of pure radiation.

Andy Weir, *The Martian*

4 Results

The goal of this chapter is to explore this model with some realistic parameters. Then, we use the model to construct a joint spectral amplitude and to predict the rate at which such a source would produce pairs of photons. We will also discuss the spontaneous Raman scattering impact on this source.

4.1 A coarse grained approach

To get a rough idea of a pair rate before resorting to numerics, in eq. (3.46) we allow the pump Gaussian to also be quite long (which is not likely to optimise the rate of pair production during an experiment), approximating $\tau_p \approx \tau_s \equiv \tau$ so that we can take $\tau \mathrm{e}^{-\frac{\tau^2}{2}\omega^2} \approx \sqrt{2\pi}\delta(\omega)$. Now, performing the ω_2 integral, we find (recall eq. (3.45))

$$\begin{aligned}|\eta|^2 \approx & \frac{|\alpha|^2 |\beta|^2 \gamma^2 \hbar^2 \omega_s^2 L^2}{\pi^2} \int_0^\infty \mathrm{d}\omega_1 \int_0^\infty \mathrm{d}\omega_2 \, \mathrm{e}^{-\frac{\tau^2}{2}(\omega_1+\omega_2-2\omega_s)^2} \operatorname{sinc}^2\left(\frac{\Delta k L}{2}\right) \\ \approx & \frac{|\alpha|^2 |\beta|^2 \gamma^2 \hbar^2 \omega_s^2 L^2}{\pi^2} \frac{\sqrt{2\pi}}{\tau} \int_0^\infty \mathrm{d}\omega_1 \int_0^\infty \mathrm{d}\omega_2 \, \delta(\omega_1+\omega_2-2\omega_s) \operatorname{sinc}^2\left(\frac{\Delta k L}{2}\right)\end{aligned}$$

We note here that the integration over the Dirac delta function has simplified the form of Δk, as it sets $\omega_2 = 2\omega_s - \omega_1$. This means that in eq. (3.45) the factors of $(\omega_1 + \omega_2 - 2\omega_s) = 0$,

leaving only the final term which simplifies to $-\beta_2(\omega_s)\,(\omega_1-\omega_s)^2$. This gives us

$$\begin{aligned}|\eta|^2 =& \frac{|\alpha|^2\,|\beta|^2\,\gamma^2\hbar^2\omega_s^2L^2\sqrt{2\pi}}{\pi^2\tau}\int_0^\infty \mathrm{d}\omega_1\ \mathrm{sinc}^2\left(\frac{\beta_2(\omega_s)\,(\omega_1-\omega_s)^2\,L}{2}\right)\\ =& \frac{2\,|\alpha|^2\,|\beta|^2\,\gamma^2\hbar^2\omega_s^2L^2\sqrt{2\pi}}{3\pi^2\tau}\sqrt{\frac{2\pi}{|\beta_2\,(\omega_s)|\,L}}\\ =& \frac{4\,|\alpha|^2\,|\beta|^2\,\gamma^2\hbar^2\omega_s^2L^2}{3\pi\tau\sqrt{|\beta_2\,(\omega_s)|\,L}},\end{aligned} \tag{4.1}$$

Finally, we transform this into an expression in terms of powers using eqs. (3.47) and (3.48). We find

$$|\eta|^2 = \frac{4\gamma^2L^2\tau}{3\pi\sqrt{|\beta_2(\omega_s)|\,L}}P_pP_s.$$

and using the results from our model (as found in table 4.2), we find that in fused silica microfibres, we can produce $|\eta|^2 = 0.01$ pairs per pulse. This is a high enough rate for an effective heralded single photon source. The rate is low enough to keep the multi-pairs at a small fraction of the produced photons ($\sim 3\%$ recalling eq. (2.24)), and with a moderate repetition rate a high rate of pairs. Indeed, it is common to work in the regime where $|\eta|^2$ is in the range $10^{-3} - 10^{-1}$.

4.1.1 Comparison with Literature

In order to verify that this method gives similar results to other work, we compare with Gravier and Boulanger (2008) [48]. Whilst their aim is to produce photon triplets, the process is similar. They use a four wave mixing process that involves the annihilation of a pump photon at ω_0 in bulk potassium titanyl phosphate (KTP) to produce photons at ω_1, ω_2 and ω_3, where $\omega_2 = \omega_3$. The corresponding wavelengths are $\lambda_0 = 532\,\mathrm{nm}$, $\lambda_1 = 1474\,\mathrm{nm}$ and $\lambda_2 = \lambda_3 = 1665\,\mathrm{nm}$. However, because this process is intrinsically slow, they also seed this generation with a field ω_2. This is described by the Hamiltonian we ignored earlier on the basis of phasematching (eq. (3.23)). Gravier and Boulanger quote a rate of 3.3×10^{13} triplets per pulse, from 2.0×10^{15} photons in their seed field, and 8.4×10^{14} photons in their pump field.

Following the same method from chapter 3, we find that this state is described by

$$|\psi_{\mathrm{out}}\rangle \approx |\mathrm{vac}\rangle + \eta_S\,|\mathrm{I}\rangle,$$

where the state of the single photon is

$$|\mathrm{I}\rangle = \frac{3i\,(\alpha^*)^2\,\beta\hbar}{32\pi\varepsilon_0\eta_S}\int_0^\infty \mathrm{d}\omega \int_0^\infty \mathrm{d}\omega_1 \int_0^\infty \mathrm{d}\omega_2 \sqrt{\frac{\omega\,\omega_1\,\omega_2\,(\omega+\omega_1+\omega_2)}{v_g(\omega)v_g(\omega_1)v_g(\omega_2)v_g(\omega+\omega_1+\omega_2)}} \times \frac{\mathfrak{s}^*\,(\Delta k)\,\bar{\chi}_3}{\bar{n}^4}\frac{\bar{\phi}_s^*(\omega_1)\bar{\phi}_s^*(\omega_2)\bar{\phi}_p(\omega+\omega_1+\omega_2)}{\mathcal{A}\,[k(\omega),k(\omega_1),k(\omega_2),k(\omega+\omega_1+\omega_2)]}\hat{a}_\omega^\dagger\,|\mathrm{vac}\rangle,$$

and

$$\Delta k = k(\omega+\omega_1+\omega_2) - k(\omega_2) - k(\omega_1) - k(\omega).$$

Now we only have a single creation operator acting on the vacuum state. Again following the same steps as above, we calcuate the average number of triple photons produced per pulse as

$$|\eta_S|^2 \approx \frac{|\alpha|^4\,|\beta|^2\,\gamma^2\hbar^2\omega_s^2L^2}{\pi^2}\int_0^\infty \mathrm{d}\omega \times \left|\int_0^\infty \mathrm{d}\omega_1 \int_0^\infty \mathrm{d}\omega_2\,\mathrm{sinc}\left(\frac{\Delta kL}{2}\right)\bar{\phi}_s^*(\omega_1)\bar{\phi}_s^*(\omega_2)\bar{\phi}_p(\omega+\omega_1+\omega_2)\right|^2.$$

Although the pulse durations in the actual experiment are $\tau_p = 106\,\mathrm{ps}$ and $\tau_s = 230\,\mathrm{ps}$, because we are only looking for rough agreement with our theory, we approximate their durations as identical and long enough to fix the arguments of the sinc function, such that

$$\begin{aligned}
|\eta_S|^2 \approx& \frac{|\alpha|^4\,|\beta|^2\,\gamma^2\hbar^2\omega_s^2L^2}{\pi^2}\frac{\tau^3}{\pi^{3/2}} \\
&\times \int_0^\infty \mathrm{d}\omega \left|\int_0^\infty \mathrm{d}\omega_1 \int_0^\infty \mathrm{d}\omega_2\,\mathrm{e}^{-\frac{1}{2}\tau^2(\omega_1-\omega_s)^2}\mathrm{e}^{-\frac{1}{2}\tau^2(\omega_2-\omega_s)^2}\mathrm{e}^{-\frac{1}{2}\tau^2\left(\omega+\omega_1+\omega_2-\omega_p\right)^2}\right|^2 \\
=& \frac{|\alpha|^4\,|\beta|^2\,\gamma^2\hbar^2\omega_s^2L^2}{\pi^2}\mathrm{sinc}^2\left(\frac{\left[k(\omega_p)-2k(\omega_s)-k(\omega_p-2\omega_s)\right]L}{2}\right)\frac{\tau^3}{\pi^{3/2}} \\
&\times \frac{4\pi^2}{3\tau^4}\int_0^\infty \mathrm{d}\omega\,\mathrm{e}^{-\frac{1}{3}\tau^2\left(\omega+2\omega_s-\omega_p\right)^2} \\
=& \frac{4\,|\alpha|^4\,|\beta|^2\,\gamma^2\hbar^2\omega_s^2L^2}{\sqrt{3}\pi\tau^2}\mathrm{sinc}^2\left(\frac{\left[k(\omega_p)-2k(\omega_s)-k(\omega_p-2\omega_s)\right]L}{2}\right).
\end{aligned} \tag{4.2}$$

In terms of powers, we predict an "idler" power of

$$P_i = \frac{4}{\sqrt{3}\pi}\gamma^2P_s^2P_pL^2\mathrm{sinc}^2\left(\frac{\left[k(\omega_p)-2k(\omega_s)-k(\omega_p-2\omega_s)\right]L}{2}\right),$$

and comparing eq. (4.1) with eq. (4.2) we find

$$\frac{|\eta_S|^2}{|\eta|^2} = \frac{|\alpha|^2}{\tau}\sqrt{3\beta_2\left(\omega_s\right)L}\mathrm{sinc}^2\left(\frac{\left[k(\omega_p) - 2k(\omega_s) - k(\omega_p - 2\omega_s)\right]L}{2}\right).$$

As we might expect, the generation rate is greater by a factor including the extra seed field due to the degenerate nature of ω_2 and ω_3.

Table 4.1: Approximate values to match the experiment in Gravier *et al.* [48]. Some of these quantities, such as the effective area, are very rough estimates based on the limited information available. We use geometric averages to find effective the pulse duration and mean group index.

Quantity	Symbol	Value
Pulse duration	τ	$\sqrt{(106\,\mathrm{ps})(230\,\mathrm{ps})}$
Interaction length	L	21 mm
Photons per seed pulse	$\lvert\alpha\rvert^2$	7×10^{14}
Photons per pump pulse	$\lvert\beta\rvert^2$	10^{16}
Seed frequency	ω_s	$\frac{2\pi c}{1665\,\mathrm{nm}}$
Pump frequency	ω_p	$\frac{2\pi c}{532\,\mathrm{nm}}$
Third order susceptibility	$\chi^{(3)}$	$10^{-21}\mathrm{m}^2/\mathrm{V}^2$
Effective area	$\mathcal{A}$	$\pi(125\,\mu\mathrm{m})^2$
Mean refractive index	$\bar{n}$	$\sqrt[4]{(1.7263)^2(1.7294)(1.7779)}$
Mean group index	$\bar{n}_g$	$\sqrt[4]{(1.7534)^2(1.7546)(1.8909)}$
Group velocity dispersion	β_2	$4.3\,\mathrm{ps}^2/\mathrm{km}$

Finally using the approximated values in table 4.1 and assuming perfect phase matching (such that $\mathrm{sinc}^2\left(\Delta kL/2\right) = 1$), we approximate the number of triplets generated per pulse, based on eq. (4.2), to be $|\eta_S|^2 \approx 1.5 \times 10^{12}$. For all of the approximations involved, being off by only an order of magnitude seems reasonable. Furthermore, for our purposes it suffices to approximate the group index n_g and group velocity dispersion β_2 by taking derivatives of the Sellmeier equation for KTP (source: refractiveindex.info $n(\alpha)$), yielding $\beta_2 = 4.3\,\mathrm{ps}^2/\mathrm{km}$. We would also approximate $|\eta|^2 \approx 21$ pairs per pulse.

4.2 A model photon source

As we cannot solve eq. (3.46) analytically, we develop a model to generate realistic parameters. There are several schemes we could consider, such as an integrated waveguide in a chalcogenide glass [20], or a silicon nitride nanowire [49]. Attempting this process over such a broad range of frequencies would be difficult in silicon, which has a small bandgap, so that the pump would be subject to both linear and nonlinear losses. For now we shall consider SSTPDC in fused silica microfibre (an air-clad, sub-micron diameter optical fibre), due to its comparatively high nonlinearity of $\chi^{(3)} = 2.5 \times 10^{-22}\,\mathrm{m^2\,V^{-2}}$, and the high refractive index contrast ($\Delta\bar{n} = 0.45$) provides high mode confinement, further enhancing the nonlinearity.

Our primary consideration is how to phasematch this process to first order, to maximise the rate of photon pair generation. We follow the process developed by Grubsky *et al.* [50], and further refined by Zhang *et al.* [35], to phasematch classical third harmonic generation. As we expect $n_{\mathrm{HE}_{11}} > n_{\mathrm{HE}_{21}}$, we pump in HE_{21} and seed in HE_{11}, to generate pairs in HE_{11}. Note that these modes in microfibre do not correspond directly to the familiar linearly polarised (LP) modes, while we no longer satisfy the condition of working with a single polarisation, we expect the error to be no greater than a factor of $\sim 50\%$. We outline a more precise approach in chapter 5.

The field amplitude profiles, generated using commercial beam propagation software (RSoft), are found in Figure 4.2. These modes have appreciable overlaps, leading to an effective coupling area of $A_{\mathrm{eff}} = 11.9\,\mu\mathrm{m}^2$. Note that we use a scalar approximation, so eq. (3.19) collapses down to a single term and we gain a factor of four. We approximate the profiles of $\mathrm{HE}_{11}(\omega_s)$, $\mathrm{HE}_{11}(\omega_1)$ and $\mathrm{HE}_{11}(\omega_2)$ as being identical. We cannot use HE_{11} and HE_{12} as HE_{12} is odd, and so the nonlinear overlap would be zero.

As the modal dispersion has a dependency on the width of the fibre, we can use the same beam propagation software to scan across fibre diameters until we find a value for which $n_{\mathrm{eff}}^{(\mathrm{HE}_{11})}(\omega_s) = n_{\mathrm{eff}}^{(\mathrm{HE}_{21})}(\omega_p)$, thereby phasematching SSTPDC to first order. As shown in Figure 4.1, this occurs for a fibre width of 765 nm. All of the remaining parameters are shown in table 4.2.

4.3 Results of the model

Using this set of parameters, we endeavour to produce photons around the 1550 nm band. We envisage pumping with $\tau_p = 1$ ps pulses at 517 nm and seeding with $\tau_s = 10$ ps pulses at 1550 nm. From eq. (3.49) we find that $|\eta|^2 = 0.01$ pairs per pulse. This is more than sufficient for producing an effective heralded photon source. Examining the joint spectral intensity as given by eq. (3.49), seen in Figure 4.3, we find that our pairs are highly correlated.

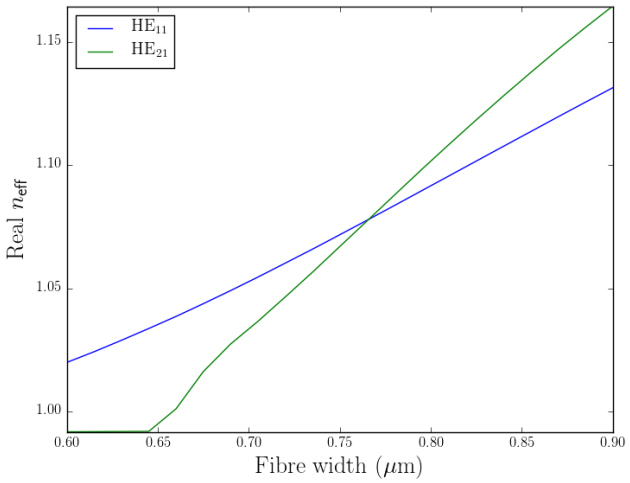

Figure 4.1: The effective refractive indices for HE_{11} and HE_{21}. Phasematching occurs when the fibre width is 765 nm.

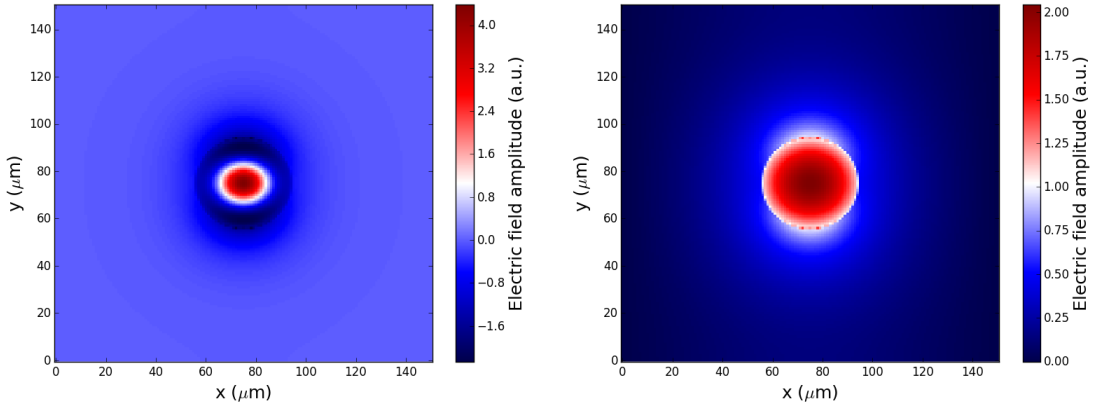

Figure 4.2: The field amplitude profiles for HE_{11}(1550 nm) (right) and HE_{21}(517 nm) (left) in a fused silica microfibre.

Recalling the discussion of separability from section 1.4.2, the shape of this joint state intensity (JSI) is described primarily by the "width" roughly along the $\omega_2 = \omega_1$ axis, the generation bandwidth (*i.e.* the "length" along the $\omega_2 = 2\omega_s - \omega_1$ axis), and the "bend" away from the $\omega_2 = 2\omega_s - \omega_1$ axis. Correspondingly these three things are controlled by the interaction length, L, the pump duration, τ_p, and the strength of the dispersion as described by $\beta_2(\omega_p) - \beta_2(\omega_s)$.

Another metric discussed in section 1.4.2 that measures the level of correlation is the Schmidt number K. We recall that $K \geq 1$, with equality only when the JSA shows no correlations (that is, for states that can be factorised as $\Phi(\omega_1, \omega_2) = f(\omega_1)g(\omega_2)$). For the numerical calculation, we can recover the Schmidt coefficients p_λ by finding the singular value decomposition (SVD) of the array representing the JSA, with the eigenvalues being

Table 4.2: The parameters for the quantum SSTPDC simulation. The group velocity and group velocity dispersion were acquired from the beam propagation method used to simulate the mode profiles.

Quantity	Symbol	Value
Refractive index	n_3	1.46
	n_4	1.44
Effective area	A_{eff}	$11.9\,\mu\text{m}^2$
Third order susceptibility	$\chi^{(3)}$	$2.5 \times 10^{-22}\text{m}^2/\text{V}^2$
Interaction length	L	3 mm
Group index	$n_g(\omega_s)$	1.426
	$n_g(\omega_p)$	1.613
Group velocity dispersion	$\beta_2(\omega_s)$	$-170\,\text{ps}^2/\text{km}$
	$\beta_2(\omega_p)$	$850\,\text{ps}^2/\text{km}$
Pulse Power	P_3	50 W
	P_4	10 kW
Wavelength	λ_3	1550 nm
	λ_4	1550/3 nm
Pulse duration	τ_s	10 ps
	τ_p	1 ps

$\sqrt{p_\lambda}$, where the normalisation of the JSA implies $\sum_\lambda p_\lambda = 1$. The Schmidt number is given by $K = 1/\sum_\lambda p_\lambda^2$. Alternatively, we can approximate the JSA as Gaussian

$$\Phi(\omega_1, \omega_2) = \sqrt{\frac{2}{\pi}}\sqrt{\frac{\cos\theta_1 \sin\theta_2 - \sin\theta_1 \cos\theta_2}{\sigma_1\sigma_2}} \times \exp\left(-\frac{(\omega_1 \sin\theta_1 + \omega_2 \cos\theta_1)^2}{\sigma_1^2}\right)\exp\left(-\frac{(\omega_1 \sin\theta_2 + \omega_2 \cos\theta_2)^2}{\sigma_2^2}\right), \quad (4.3)$$

where θ_1, θ_2 are angles determining the orientation of the JSA, and σ_1, σ_2 the widths along the respective directions determined by the orientation. This allows one to find the following analytical expression for the Schmidt number in this approximation [51]

$$K = \sqrt{\frac{\left(\sigma_1^2 \sin^2\theta_2 + \sigma_2^2 \sin^2\theta_1\right)\left(\sigma_1^2 \cos^2\theta_2 + \sigma_2^2 \cos^2\theta_1\right)}{\sigma_1^2\sigma_2^2\left(\cos\theta_1 \sin\theta_2 - \sin\theta_1 \cos\theta_2\right)^2}}. \quad (4.4)$$

Clearly, some of the joint state intensities shown in fig. 4.4 are not well approximated by a Gaussian. Thus we use the Gaussian approximation only to verify the numerical result in the case of fig. 4.3, where $\theta_1 = -\pi/4, \theta_2 = \pi/4$, and $\sigma_1/\sigma_2 = 50$. We find $K_{\text{Gauss}} = 25.01$, compared with the numerical result $K_{\text{SVD}} = 26.6$ – suggesting that the SVD is producing a trustworthy Schmidt number.

To illustrate how the correlations are affected by the parameter space, we consider several

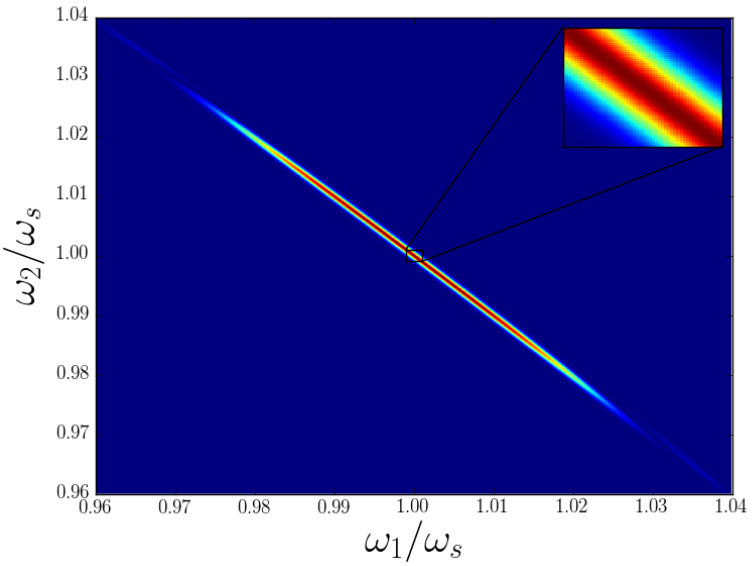

Figure 4.3: The normalised joint spectral intensity for SSTPDC in fused silica microfibre, with a Schmidt number of $K = 26.6$, and a rate $|\eta|^2 = 0.01$ pairs per pulse.

cases. First we decrease the pump duration to $\tau_p = 0.1$ ps, resulting in Figure 4.4b. As we can see, this has extended the generation bandwidth (note the broader frequency range), and made the effect of dispersion more pronounced. This makes sense, as we have broadened the Gaussian term in the $\omega_2 = \omega_1$ direction, so it overlaps with more of the sinc. We see that the Schmidt number has increased to $K = 34.4$, meaning this source shows greater correlations than fig. 4.3, and the rate has decreased to $|\eta|^2 = 7 \times 10^{-4}$ pairs per pulse. If we increase the pulse width by even a factor of two, to 2 ps, the result is barely resolvable. With the constraint that $\tau_s \ll \tau_p$, this behaviour is always dominated by the pump pulse duration. Next, we exaggerate the second order dispersion by increasing $\beta_2(\omega_p)$ and $\beta_2(\omega_s)$ by a factor of four (this might be accomplished by using a smaller waveguide). This has caused the $\mathrm{sinc}(\Delta kL/2)$ to "bend" further from the $\omega_2 = -\omega_1 + 2\omega_s$ axis and overlap less with the Gaussian, as seen in Figure 4.4c. This effectively shortens the generation bandwidth. However, it has also decreased the Schmidt number to $K = 13.5$, and the rate has only decreased slightly to $|\eta|^2 = 0.007$ pairs per pulse. Finally, we double the interaction length to 6 mm, giving us Figure 4.4d. Primarily this has narrowed the "width" of the JSI, but we also see a slightly increase in the Schmidt number to $K = 30.4$, and an increase in the rate to $|\eta|^2 = 0.04$ pairs per pulse.

Another quantity related to the correlations in the source is the second-order correlation function, $g^{(2)}$. Unlike the form in section 1.4.1, here we consider a $g^{(2)}$ pertaining to

multimode squeezed states

$$g^{(2)} = 1 + \frac{\sum_\lambda \sinh^4(r_\lambda)}{\left[\sum_\lambda \sinh^2(r_\lambda)\right]^2}, \tag{4.5}$$

where $r_\lambda = |\eta|^2 \sqrt{p_\lambda}$, with $\sqrt{p_\lambda}$ being the eigenvalues given by the SVD. In the limit where $|\eta|^2 \ll 1$, this reduces to

$$g^{(2)} = 1 + \frac{1}{K}. \tag{4.6}$$

This tells us then that for an uncorrelated heralded single photon source, we should expect $g^{(2)} = 2$. If there are very strong frequency correlations overall, then the Schmidt number is large, and we are likely to get two successive photons from different modes. As they are in different modes, they are uncorrelated, and these events happen independently. Thus the arrival of successive photons should be described by Poisson statistics, *i.e.* $g^{(2)} \to 1$.

The temporal form of the JSI (*i.e.* $|\phi(t_1, t_2)|^2 = \left|\frac{1}{2\pi}\int \mathrm{d}\omega_1 \mathrm{d}\omega_2 \phi(\omega_1, \omega_2) e^{i(\omega_1 t_1 + \omega_2 t_2)}\right|^2$) is shown in Figure 4.5. This clearly shows that we have temporal correlations, as well as the spectral correlations we see in Figure 4.3. We can see here that the temporal bandwidth is narrow, with pair generation occurring over a range on the order of 6 ps. This suggests that in order to generate pure states, we would need a detector with a response time on the order of 1 ps. This is infeasible, filtering would be required. Alternatively, performing the calculation in a ring resonator may result in a state that is closer to separable [52].

In this treatment we have not explicitly accounted for the effect of spontaneous Raman scattering, but we can comment on the impact on this source regardless. The number of Raman photons produced per second is linearly proportional to the pulse power, $|\eta_\mathrm{R}|^2 \propto \gamma P_0 L$ [29] (assuming our filtering is narrower than the Stokes bandwidth which is approximately 20 THz), with the specifics depending on the material and configuration. Here, the seed laser near the produced pairs is extremely weak in comparison to the pump field (by a very large factor of $\sim 10^8$). It is clear then that the vast majority of Raman photons will be produced around the pump field, with enough spectral separation between it and the pump for cascaded processes to irrelevant in the spontaneous regime. We compare this with the pump power used by Clark *et al.* [19] in their birefringent photonic crystal fibre SFWM source, which uses a pulse power of approximately 5 kW to produce pairs only 30 nm away from their pump, more than 10^5 times the pulse power in the seed pulse used for SSTPDC. This suggests that there should be a significant decrease in Raman noise when producing pairs via SSTPDC.

Not all of these results are ideal – for example, we do not demonstrate the ability to produce an uncorrelated source. However, the parameter space is large enough that there is significant room for further optimisation. Furthermore, this is a simple proof of principle. One could consider other platforms and geometries that produce different results.

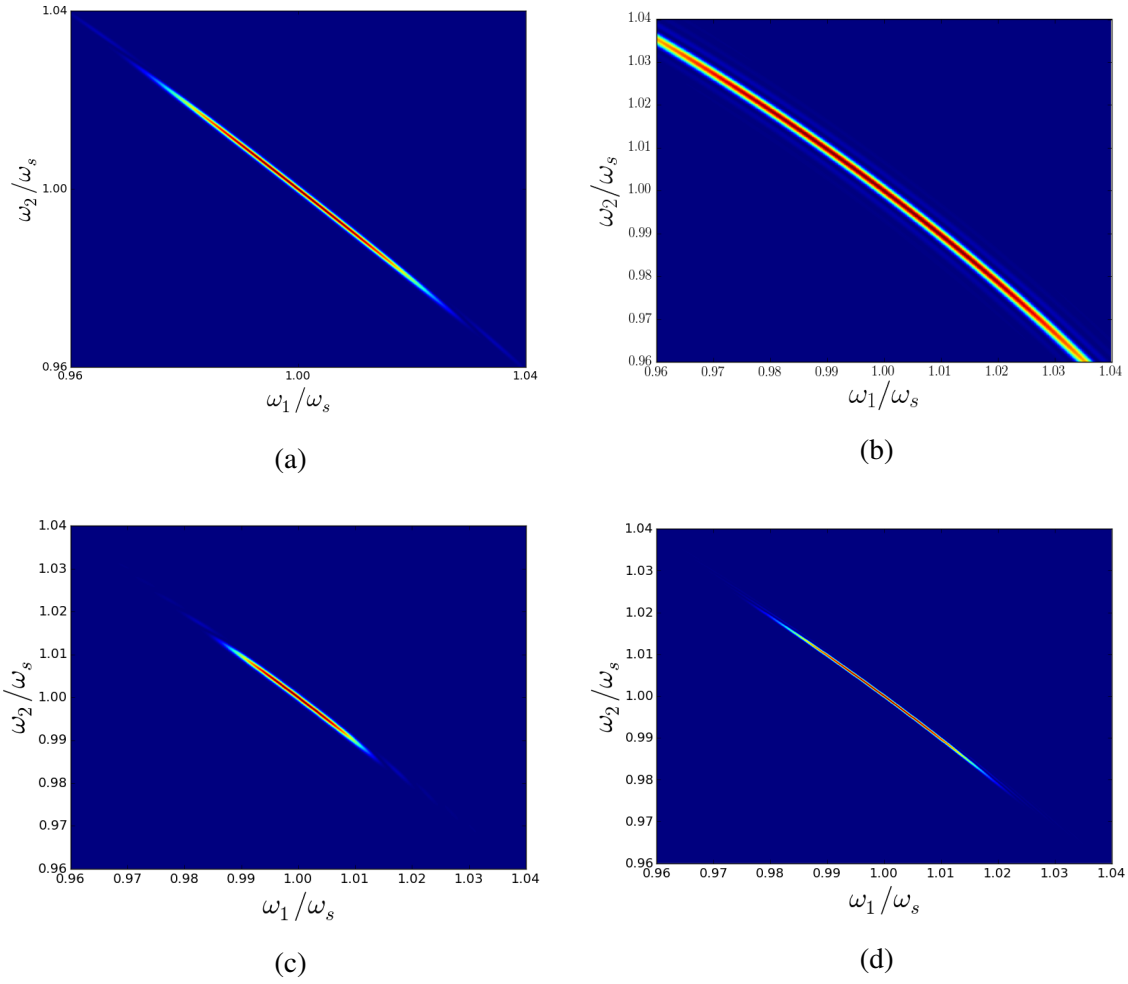

Figure 4.4: The normalised joint spectral intensity for **(a):** the JSI from fig. 4.3 for comparison. **(b):** a pump duration of 0.1 ps. Note that the generation bandwidth has increased such that it no longer fits in the same interval. For the entire JSA, $K = 34.4$, $g^{(2)} = 1.03$. The rate has decreased to $|\eta|^2 = 7 \times 10^{-4}$ pairs per pulse. **(c):** a four fold increase in the group velocity dispersion. Now $K = 13.5$, $g^{(2)} = 1.07$, and the rate is $|\eta|^2 = 0.007$ pairs per pulse. **(d):** an interaction length of 6 mm. Here $K = 30.4$, $g^{(2)} = 1.03$, and $|\eta|^2 = 0.04$ pairs per pulse.

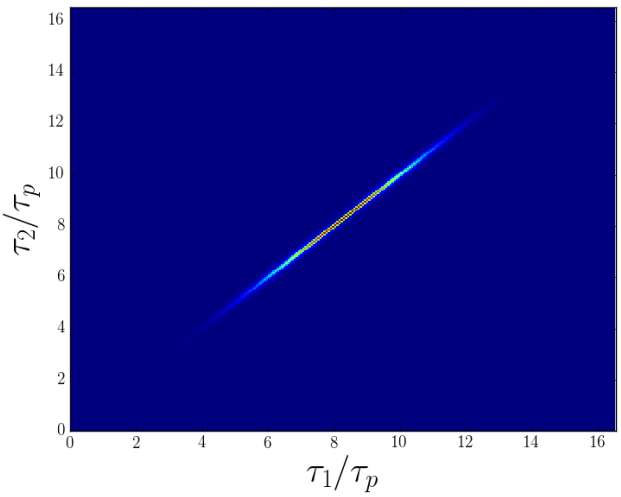

Figure 4.5: The temporal form of the biphoton function.

The Universe is making music all of the time.

Tom Waits

5 Outlook

In this thesis, we have established that one of the key difficulties facing nonlinear optical heralded single photon sources is noise due to spontaneous Raman scattering in amorphous materials. Because these materials lend themselves well to integrated optics, and we would like to take advantage of the inherent stability and scalability of this integration, Raman noise is a problem that must be addressed.

Our proposed solution is the third-order nonlinear process Stimulated Spontaneous Three Photon Down Conversion. The issue of Raman noise is side-stepped by simply having a large spectral separation between the strong noise source (the pump) and the generated pairs. By comparison with the semi-classical analogue in section 2.2, we have shown that even with nonlinear contributions from self and cross phase modulation, this process can be phasematched. Furthermore, section 2.3 establishes that this process does in fact generate pairs by lightly squeezing the vacuum, in much the same way as spontaneous parametric down conversion or degenerate four wave mixing.

The bulk of our work here is dedicated to describing SSTPDC in its entirety, for which we have relied upon the robust backwards Heisenberg formalism pioneered by Yang *et al.* (2008) [40]. In principle this approach can describe a process of any order, but here we have only extracted the physics relevant to our third order down conversion process. The full theory behind SSTPDC is fleshed out in chapter 3, and we arrive at very general equations describing both the biphoton state (eq. (3.35)) and the pair generation rate (eq. (3.39)).

It is important to realise that the joint spectral amplitude described by eq. (3.35) is a complete characterisation of the biphoton state, provided we work in the low power regime where time-ordering effects are negligible. Any information that we might wish to find can be calculated from the JSA. This includes, as we have seen, the Schmidt number and second-order correlation function.

In the previous chapter (chapter 4), we developed a model in fused silica microfibre. We demonstrated the ability to produce pairs of photons at 0.01 pairs per pulse, a sufficiently high rate for an SSTPDC based heralded single photon source to be effective. This source is highly correlated, with a Schmidt number of $K = 26.6$. For applications such as multichannel QKD [53–55], this is a promising result. As of yet we have not demonstrated the ability to generate pure states without tight filtering, but SSTPDC has a large parameter space and we have explored only a single platform. The impact of spontaneous Raman scattering on this source was considered briefly, which suggested that there was a reduction in the number of Raman photons produced proportional to the pump power. As SSTPDC only needs a weak seed near the pair generation band, we expect a significant reduction in noise.

There are further effects to consider that have not been accounted for in this treatment. The three primary ones are cross-phase modulation, self-phase modulation, and the single polarisation approximation. These all add further complexity to this treatment of SSTPDC.

Self and cross phase modulation are particularly relevant here, as our pump pulse durations are on the order of picoseconds. These effects are going to modulate the spectral profiles of the pulses, and contribute to the phasematching, as we saw in section 2.2. It would be ideal to confirm that in this Hamiltonian treatment of the spontaneous problem, these effects are negligible. One strategy for attempting this is to work in the time domain, where calculations of these type can be simplified [56].

Another concern is the use of the scalar approximation to calculate the effective area in chapter 4. This approximation is not a particularly good one in microfibre, where every polarisation component has a significant field contribution. However, we expect the improvement in accuracy in using the full tensorial form described by eq. (3.19) to be of order $\sim 50\%$. The $\chi^{(3)}$ tensor in amorphous materials has few independent elements, however we must determine the appropriate symmetries for SSTPDC, as well as the relevant frequency dependence.

Despite the theoretical nature of this thesis, we have in effect designed a source which one could construct in the laboratory. The one major practical consideration left uncommented on here is the necessary filtering one would require to undertake such an experiment – this will necessarily lower the rate.

Ultimately we have demonstrated that by this third order process we call Stimulated Spontaneous Three Photon Down Conversion, where we down convert a pump photon at the

third harmonic to a triplet around the fundamental frequency, and stimulate this process with a seed at the frequency of one of the triplet photons, one can in principle generate 0.01 pairs per pulse using modest laser powers. Taking into account more realistic laser fields we still find a rate of 0.01 pairs per pulse, for the pulse powers of $P_s = 50\,\mathrm{W}$ and $P_p = 10\,\mathrm{kW}$ for the seed and pump, respectively. This rate is sufficient to produce an effective heralded single photon source for many applications. Importantly, as the desired pairs have been spectrally separated from the strongest pump field, we expect a significant decrease in the rate of uncorrelated photons generated by spontaneous Raman scattering. Stimulated spontaneous three photon down conversion then is a good candidate for a correlated heralded single photon source.

A

Appendix

A.1 From χ to Γ

It is, on occasion, useful to know the relationship between χ and Γ [57]. This is because χ is the quantity that is tabulated and printed in reference books. For the linear susceptibility, this is easy. If

$$P^i = \epsilon_0 \chi^{(1)}_{ij} E^j = \chi^{(1)}_{ij} \left(D^j - \Gamma^{(1)}_{jl} D^l \right)$$

and

$$P^i = \Gamma^{(1)}_{ij} D^j$$

then we can solve for $\Gamma^{(1)}$ in terms of $\chi^{(1)}$. Assuming that we are working in an isotropic medium, meaning $\chi^{(1)}_{ij} = \chi^{(1)} \delta_{ij}$ and $\Gamma^{(1)}_{ij} = \Gamma^{(1)} \delta_{ij}$, we find

$$\Gamma^{(1)} = \frac{\chi^{(1)}}{1 + \chi^{(1)}} = \frac{n_0^2 - 1}{n_0^2}, \tag{A.1}$$

where n_0 is the material refractive index.

The process for the second order is more involved. Now we use

$$\begin{aligned} P^i &= \epsilon_0 \chi^{(1)}_{ij} E^j + \epsilon_0 \chi^{(2)}_{ijm} E^j E^m \\ &= \chi^{(1)}_{ij} \left(D^j - \Gamma^{(1)}_{jl} D^l - \Gamma^{(2)}_{jlm} D^l D^m \right) + \frac{\chi^{(2)}_{ijm}}{\epsilon_0} \left(D^j - \Gamma^{(1)}_{jl} D^l \right) \left(D^m - \Gamma^{(1)}_{mn} D^n \right) \end{aligned}$$

and

$$P^i = \Gamma^{(1)}_{ij} D^j + \Gamma^{(2)}_{ijm} D^j D^m$$

to find that

$$\Gamma^{(2)}_{ijm} = \frac{\chi^{(2)}_{ijm}}{\epsilon_0 n_0^6}. \tag{A.2}$$

The third order relationship is worse again. However, carefully managing indices, we can use

$$\begin{aligned} P^i =& \epsilon_0 \chi^{(1)}_{ij} E^j + \epsilon_0 \chi^{(2)}_{ijm} E^j E^m + \epsilon_0 \chi^{(3)}_{ijmn} E^j E^m E^n \\ =& \chi^{(1)}_{ij} \left(D^j - \Gamma^{(1)}_{jl} D^l - \Gamma^{(2)}_{jlm} D^l D^m - \Gamma^{(3)}_{jlmn} D^l D^m D^n \right) \\ &+ \frac{\chi^{(2)}_{ijm}}{\epsilon_0} \left(D^j - \Gamma^{(1)}_{jl} D^l - \Gamma^{(2)}_{jlm} D^l D^m \right) \left(D^m - \Gamma^{(1)}_{mn} D^n - \Gamma^{(2)}_{mnp} D^n D^p \right) \\ &+ \frac{\chi^{(3)}_{ijmn}}{\epsilon_0^2} \left(D^j - \Gamma^{(1)}_{jl} D^l \right) \left(D^m - \Gamma^{(1)}_{mn} D^n \right) \left(D^n - \Gamma^{(1)}_{np} D^p \right) \end{aligned}$$

and

$$P^i = \Gamma^{(1)}_{ij} D^j + \Gamma^{(2)}_{ijm} D^j D^m + \Gamma^{(3)}_{ijmn} D^j D^m D^n$$

in order to find

$$\Gamma^{(3)}_{ijlm} = \frac{\chi^{(3)}_{ijlm}}{\epsilon_0^2 n_0^8}. \tag{A.3}$$

A.2 The Linear Hamiltonian

The electric inhomogeneous linear part of our Hamiltonian takes the following form,

$$\hat{H}_L = \frac{1}{2\epsilon_0} \int \mathrm{d}\mathbf{r} \, \frac{\hat{D}^i \hat{D}^i}{n^2}. \tag{A.4}$$

We now follow much the same process as in Section 3.1 using eqs. (3.7), (3.9) and (3.10). We must be careful to keep track of the frequency and spatial dependence of the refractive

indices of each field. This gives us

$$\hat{H}_L = \frac{1}{2\epsilon_0}\int \mathrm{d}\mathbf{r}\int_0^\infty \mathrm{d}k_1\int_0^\infty \mathrm{d}k_2\,\frac{1}{n_{k_1}n_{k_2}}\sqrt{\frac{\hbar\omega_{k_1}}{2}}\sqrt{\frac{\hbar\omega_{k_2}}{2}} \left[D_{k_1}\hat{a}_{k_1}+F_{k_1}\hat{b}_{k_1}+D^*_{k_1}\hat{a}^\dagger_{k_1}+F^*_{k_1}\hat{b}^\dagger_{k_1}\right]\times\left[D_{k_2}\hat{a}_{k_2}+F_{k_2}\hat{b}_{k_2}+D^*_{k_2}\hat{a}^\dagger_{k_2}+F^*_{k_2}\hat{b}^\dagger_{k_2}\right] \tag{A.5}$$

Now we simply expand;

$$\begin{aligned}\hat{H}_L = \frac{\hbar}{4\epsilon_0}\int \mathrm{d}\mathbf{r}\int_0^\infty \mathrm{d}k_1\int_0^\infty \mathrm{d}k_2\,\frac{\sqrt{\omega_{k_1}\omega_{k_2}}}{n_{k_1}n_{k_2}} &\Big[F_{k_1}F_{k_2}\hat{b}_{k_1}\hat{b}_{k_2}+D_{k_1}D_{k_2}\hat{a}_{k_1}\hat{a}_{k_2}+F^*_{k_1}F^*_{k_2}\hat{b}^\dagger_{k_1}\hat{b}^\dagger_{k_2}+D^*_{k_1}D^*_{k_2}\hat{a}^\dagger_{k_1}\hat{a}^\dagger_{k_2}\\ &+F_{k_1}D_{k_2}\hat{b}_{k_1}\hat{a}_{k_2}+F^*_{k_1}D^*_{k_2}\hat{b}^\dagger_{k_1}\hat{a}^\dagger_{k_2}+D^*_{k_1}F^*_{k_2}\hat{a}^\dagger_{k_1}\hat{b}^\dagger_{k_2}+D^*_{k_1}F^*_{k_2}\hat{a}^\dagger_{k_1}\hat{b}^\dagger_{k_2}\\ &+F^*_{k_1}F_{k_2}\hat{b}^\dagger_{k_1}\hat{b}_{k_2}+D^*_{k_1}F_{k_2}\hat{a}^\dagger_{k_1}\hat{b}_{k_2}+F^*_{k_1}D_{k_2}\hat{b}^\dagger_{k_1}\hat{a}_{k_2}+D^*_{k_1}D_{k_2}\hat{a}^\dagger_{k_1}\hat{a}_{k_2}\\ &+F_{k_1}F^*_{k_2}\hat{b}_{k_1}\hat{b}^\dagger_{k_2}+D_{k_1}F^*_{k_2}\hat{a}_{k_1}\hat{b}^\dagger_{k_2}+F_{k_1}D^*_{k_2}\hat{b}_{k_1}\hat{a}^\dagger_{k_2}+D_{k_1}D^*_{k_2}\hat{a}_{k_1}\hat{a}^\dagger_{k_2}\Big].\end{aligned} \tag{A.6}$$

A similar contribution from the magnetic component cancels many of these terms to leave us with

$$\begin{aligned}\hat{H}_L = \frac{\hbar}{4\pi\epsilon_0}\int \mathrm{d}\mathbf{r}\int_0^\infty \mathrm{d}k_1\int_0^\infty \mathrm{d}k_2\,\frac{\sqrt{\omega_{k_1}\omega_{k_2}}}{n_{k_1}n_{k_2}} &\Big[F^*_{k_1}F_{k_2}\hat{b}^\dagger_{k_1}\hat{b}_{k_2}+D^*_{k_1}F_{k_2}\hat{a}^\dagger_{k_1}\hat{b}_{k_2}+F^*_{k_1}D_{k_2}\hat{b}^\dagger_{k_1}\hat{a}_{k_2}+D^*_{k_1}D_{k_2}\hat{a}^\dagger_{k_1}\hat{a}_{k_2}\\ &+F_{k_1}F^*_{k_2}\hat{b}_{k_1}\hat{b}^\dagger_{k_2}+D_{k_1}F^*_{k_2}\hat{a}_{k_1}\hat{b}^\dagger_{k_2}+F_{k_1}D^*_{k_2}\hat{b}_{k_1}\hat{a}^\dagger_{k_2}+D_{k_1}D^*_{k_2}\hat{a}_{k_1}\hat{a}^\dagger_{k_2}\Big].\end{aligned} \tag{A.7}$$

Again, as we are ultimately going to be working in a waveguide, we use eq. (3.15) plus the equivalent term for our high frequency components. This will give us the following;

$$\begin{aligned}\hat{H}_L = \frac{\hbar}{8\pi\epsilon_0}\int_{-\infty}^\infty \mathrm{d}\mathbf{r}\int_0^\infty \mathrm{d}k_1\int_0^\infty \mathrm{d}k_2\,\frac{\sqrt{\omega_{k_1}\omega_{k_2}}}{n_{k_1}n_{k_2}} &\Big[e^{i(k_1-k_2)z}f^*_{k_1}f_{k_2}\hat{b}^\dagger_{k_1}\hat{b}_{k_2}+e^{i(k_1-k_2)z}f_{k_2}\hat{a}^\dagger_{k_1}\hat{b}_{k_2}\\ &+e^{i(k_1-k_2)z}f^*_{k_1}d_{k_2}\hat{b}^\dagger_{k_1}\hat{a}_{k_2}+e^{i(k_1-k_2)z}{d_{k_1}}^*d_{k_2}\hat{a}^\dagger_{k_1}\hat{a}_{k_2}+e^{-i(k_1-k_2)z}f_{k_1}f^*_{k_2}\hat{b}_{k_1}\hat{b}^\dagger_{k_2}\\ &+e^{-i(k_1-k_2)z}d_{k_1}f^*_{k_2}\hat{a}_{k_1}\hat{b}^\dagger_{k_2}+e^{-i(k_1-k_2)z}f_{k_1}{d_{k_2}}^*\hat{b}_{k_1}\hat{a}^\dagger_{k_2}+e^{-i(k_1-k_2)z}d_{k_1}{d_{k_2}}^*\hat{a}_{k_1}\hat{a}^\dagger_{k_2}\Big].\end{aligned} \tag{A.8}$$

If we now integrate with respect to the longitudinal axis, z, we find our exponentials

become Dirac delta functions;

$$\begin{aligned}\hat{H}_L = \frac{\hbar}{4\epsilon_0}\int_{-\infty}^{\infty}\int_{-\infty}^{\infty}\mathrm{d}x\,\mathrm{d}y\int_0^{\infty}\mathrm{d}k_1\int_0^{\infty}\mathrm{d}k_2\,\frac{\sqrt{\omega_{k_1}\omega_{k_2}}}{n_{k_1}n_{k_2}}\Big[&\delta(k_1-k_2)f^*_{k_1}f_{k_2}\hat{b}^\dagger_{k_1}\hat{b}_{k_2}+\delta(k_1-k_2){d_{k_1}}^*f_{k_2}\hat{a}^\dagger_{k_1}\hat{b}\\ &+\delta(k_1-k_2)f^*_{k_1}d_{k_2}\hat{b}^\dagger_{k_1}\hat{a}_{k_2}+\delta(k_1-k_2){d_{k_1}}^*d_{k_2}\hat{a}^\dagger_{k_1}\hat{a}_{k_2}+\delta(k_1-k_2)f_{k_1}f^*_{k_2}\hat{b}_{k_1}\hat{b}^\dagger_{k_2}\\ &+\delta(k_1-k_2)d_{k_1}f^*_{k_2}\hat{a}_{k_1}\hat{b}^\dagger_{k_2}+\delta(k_1-k_2)f_{k_1}{d_{k_2}}^*\hat{b}_{k_1}\hat{a}^\dagger_{k_2}+\delta(k_1-k_2)d_{k_1}{d_{k_2}}^*\hat{a}_{k_1}\hat{a}^\dagger_{k_2}\Big]\end{aligned} \tag{A.9}$$

This allows us to eliminate one of our integrals, and it is now pointless to maintain the subscript on the k;

$$\begin{aligned}\hat{H}_L = \frac{\hbar}{4\epsilon_0}\int_{-\infty}^{\infty}\mathrm{d}x\int_{-\infty}^{\infty}\mathrm{d}y\int_0^{\infty}\mathrm{d}k\,\frac{\omega_k}{n_k^2}\Big[&f^*_kf_k\hat{b}^\dagger_k\hat{b}_k+d^*_kf_k\hat{a}^\dagger_k\hat{b}_k\\ &+f^*_kd_k\hat{b}^\dagger_k\hat{a}_k+d^*_kd_k\hat{a}^\dagger_k\hat{a}_k+f_kf^*_k\hat{b}_k\hat{b}^\dagger_k\\ &+d_kf^*_k\hat{a}_k\hat{b}^\dagger_k+f_kd^*_k\hat{b}_k\hat{a}^\dagger_k+d_kd^*_k\hat{a}_k\hat{a}^\dagger_k\Big]\end{aligned} \tag{A.10}$$

It now becomes clear that, given the frequency discrimination between $\hat{b}_k$ and $\hat{a}_k$, any mixed terms are going to operate on any state to give us zero. Furthermore, we use our normalisation condition to get to the following:

$$\hat{H}_L = \int_0^{\infty}\mathrm{d}k\,\frac{\hbar\omega_k}{4}\left[\hat{b}^\dagger_k\hat{b}_k+\hat{a}^\dagger_k\hat{a}_k+\hat{b}_k\hat{b}^\dagger_k+\hat{a}_k\hat{a}^\dagger_k\right]. \tag{A.11}$$

This is an expression that we can use, although we still need to find a missing factor of two. In the process we shall verify that this is indeed the correct expression. First, we recall eqs. (3.9) and (3.10) to return to

$$\hat{H}_L = \int_0^{\infty}\mathrm{d}k\,\frac{\hbar\omega_k}{4}\left[a^\dagger_ka_k+a_ka^\dagger_k\right]. \tag{A.12}$$

Using our commutation relation $[a_k, a_{k'}] = \delta(k-k')$, we arrive at our familiar linear result, sans a factor of two:

$$\hat{H}_L = \int_0^{\infty}\mathrm{d}k\,\frac{\hbar\omega_k}{2}\left[a^\dagger_ka_k+\frac{1}{2}\right].$$

If we now include the magnetic term, we find a similar term and we have our linear Hamiltonian:

$$\hat{H}_L = \int_0^{\infty}\mathrm{d}k\,\hbar\omega_k\left[a^\dagger_ka_k+\frac{1}{2}\right]. \tag{A.13}$$

At this stage we account for the different modes in use, so the full linear Hamiltonian then

is

$$\hat{H}_{\mathrm{L}} = \int_0^\infty \mathrm{d}k\, \hbar \left[\omega_k^{(\mathrm{HE}_{11})} \hat{a}_k^\dagger \hat{a}_k + \omega_k^{(\mathrm{HE}_{21})} \hat{b}_k^\dagger \hat{b}_k \right].$$

A.3 General results

In this section, we generalise a result from Louisell [58].

Firstly we define the function

$$g(\chi) = e^{\chi \hat{I}} \hat{a}_{k_1} e^{-\chi \hat{I}}, \tag{A.14}$$

where $\chi = it$, $\hat{I} = \int_0^\infty \mathrm{d}k'\, \omega_{k'} \hat{a}_{k'}^\dagger \hat{a}_{k'}$, and we note that $g(0) = \hat{a}_{k_1}$.

If we differentiate this function, we discover

$$\frac{\mathrm{d}g}{\mathrm{d}\chi} = e^{\chi \hat{I}} \left[\hat{I}, \hat{a}_{k_1} \right] e^{-\chi \hat{I}}. \tag{A.15}$$

Simplifying this further, we find a more useful form;

$$\begin{aligned} \left[\hat{I}, \hat{a}_{k_1} \right] &= \int_0^\infty \mathrm{d}k'\, \omega_{k'} \left[\hat{a}_{k'}^\dagger \hat{a}_{k'}, \hat{a}_{k_1} \right] \\ &= \int_0^\infty \mathrm{d}k'\, \omega_{k'} \left[\hat{a}_{k'}^\dagger, \hat{a}_{k_1} \right] \hat{a}_{k'} \\ &= \int_0^\infty \mathrm{d}k'\, \omega_{k'} \left(-\delta(k' - k_1) \right) \hat{a}_{k'} \\ &= -\omega_{k_1} \hat{a}_{k_1}. \end{aligned} \tag{A.16}$$

Substituting eq. (A.16) back into eq. (A.15), we find a differential equation for $g(\chi)$;

$$\frac{\mathrm{d}g}{\mathrm{d}\chi} = -\omega_{k_1} g(\chi).$$

Combined with our initial condition, this has the solution

$$g(\chi) = \hat{a}_{k_1} e^{-\omega_{k_1} \chi}. \tag{A.17}$$

Following the same process, we can show that

$$e^{\chi \hat{I}} \hat{a}_{k_1}^\dagger e^{-\chi \hat{I}} = \hat{a}_{k_1}^\dagger e^{\omega_{k_1} \chi}. \tag{A.18}$$

References

[1] P. Kok, W. J. Munro, K. Nemoto, T. C. Ralph, J. P. Dowling, and G. J. Milburn, "Linear optical quantum computing with photonic qubits," Rev. Mod. Phys. **79**, 135–174 (2007).

[2] A. K. Ekert, "Quantum Cryptography Based on Bell's Theorem," Phys. Rev. Lett. **67**, 661–663 (1991).

[3] H. Lee, P. Kok, N. J. Cerf, and J. P. Dowling, "Linear optics and projective measurements alone suffice to create large-photon-number path entanglement," Phys. Rev. A **65**, 030101:1–4 (2001).

[4] B. Darquié, M. P. a. Jones, J. Dingjan, J. Beugnon, S. Bergamini, Y. Sortais, G. Messin, a. Browaeys, and P. Grangier, "Controlled single-photon emission from a single trapped two-level atom." Science **309**, 454–456 (2005).

[5] K. Hennessy, a. Badolato, M. Winger, D. Gerace, M. Atatüre, S. Gulde, S. Fält, E. L. Hu, and A. Imamoğlu, "Quantum nature of a strongly coupled single quantum dot-cavity system," Nature **445**, 896–899 (2007).

[6] R. Albrecht, A. Bommer, C. Pauly, F. Mücklich, A. W. Schell, P. Engel, T. Schröder, O. Benson, J. Reichel, and C. Becher, "Narrow-band single photon emission at room temperature based on a single nitrogen-vacancy center coupled to an all-fiber-cavity," Appl. Phys. Lett. **105**, 073113:1–4 (2014).

[7] S. Scheel, "Single-photon sources–an introduction," J. Mod. Opt. **56**, 141–160 (2009).

[8] D. Yu, "Single-photon emitter based on an ensemble of lattice-trapped interacting atoms," Phys. Rev. A **89**, 063809:1–9 (2014).

[9] C. Santori, D. Fattal, J. Vucković, G. S. Solomon, and Y. Yamamoto, "Indistinguishable photons from a single-photon device," Nature **419**, 594–597 (2002).

[10] C. Kurtsiefer, S. Mayer, P. Zarda, and H. Weinfurter, "Stable solid-state source of single photons," Phys. Rev. Lett. **85**, 290–293 (2000).

[11] C. Wang, C. Kurtsiefer, H. Weinfurter, and B. Burchard, "Single photon emission from SiV centres in diamond produced by ion implantation," J. Phys. B **39**, 37–41 (2006).

[12] T. H. Maiman, "Stimulated Optical Radiation in Ruby," Nature **187**, 493–494 (1960).

[13] M. G. Raymer and J. Mostowski, "Stimulated Raman scattering: Unified treatment of spontaneous initiation and spatial propagation," Phys. Rev. A **24**, 1980–1993 (1981).

[14] T. Meany, S. Gross, N. Jovanovic, A. Arriola, M. J. Steel, and M. J. Withford, "Towards low-loss lightwave circuits for non-classical optics at 800 and 1,550 nm," Appl. Phys. A **114**, 113–118 (2014).

[15] R. W. Boyd, *Nonlinear Optics* (Elsevier Science Publishing Co Inc, 2008), 3rd ed.

[16] L. A. Ngah, O. Alibart, L. Labonté, V. D. Auria, and S. Tanzilli, "Ultra-fast heralded single photon source based on telecom technology and non-linear optics," in "CLEO:2015," (2015), p. FM2A.8.

[17] X. Y. Li, P. L. Voss, J. E. Sharping, and P. Kumar, "Optical-fiber source of polarization-entangled photons in the 1550 nm telecom band," Phys. Rev. Lett. **94**, 53601:1–4 (2005).

[18] A. R. McMillan, J. Fulconis, M. Halder, C. Xiong, J. G. Rarity, and W. J. Wadsworth, "Narrowband high-fidelity all-fibre source of heralded single photons at 1570 nm," Opt. Express **17**, 6156–6165 (2009).

[19] A. Clark, B. Bell, J. Fulconis, M. M. Halder, B. Cemlyn, O. Alibart, C. Xiong, W. J. Wadsworth, and J. G. Rarity, "Intrinsically narrowband pair photon generation in microstructured fibres," New J. Phys. **13**, 065009:1–21 (2011).

[20] C. Xiong, G. D. Marshall, A. Peruzzo, M. Lobino, a. S. Clark, D. Y. Choi, S. J. Madden, C. M. Natarajan, M. G. Tanner, R. H. Hadfield, S. N. Dorenbos, T. Zijlstra, V. Zwiller, M. G. Thompson, J. G. Rarity, M. J. Steel, B. Luther-Davies, B. J. Eggleton, and J. L. O'Brien, "Generation of correlated photon pairs in a chalcogenide As_2S_3 waveguide," Appl. Phys. Lett. **98**, 051101:3–6 (2011).

[21] M. D. Birowosuto, A. Yokoo, G. Zhang, K. Tateno, E. Kuramochi, H. Taniyama, M. Takiguchi, and M. Notomi, "Movable high-Q nanoresonators realized by semiconductor nanowires on a Si photonic crystal platform," Nature Materials **13**, 279–285 (2014).

[22] J. B. Spring, P. S. Salter, B. J. Metcalf, P. C. Humphreys, M. Moore, N. Thomas-Peter, M. Barbieri, X.-M. Jin, N. K. Langford, W. S. Kolthammer, M. J. Booth, and I. a. Walmsley, "On-chip low loss heralded source of pure single photons," Opt. Express **21**, 13522:1–11 (2013).

[23] Z. Yan, Y. Duan, L. G. Helt, M. Ams, M. J. Withford, and M. J. Steel, "On-chip High Spectral Purity and Brightness Idler Single-Photon Source," in "CLEO Europe," (2015), p. JSV_1_4.

[24] C. Xiong, C. Monat, A. S. Clark, C. Grillet, G. D. Marshall, M. J. Steel, J. Li, L. O'Faolain, T. F. Krauss, J. G. Rarity, and B. J. Eggleton, "Slow-light Enhanced Correlated Photon-Pair Generation in Silicon," Opt. Lett. **36**, 3413–3415 (2011).

[25] J. Carolan, C. Harrold, C. Sparrow, E. Martín-lópez, N. J. Russell, J. W. Silverstone, P. J. Shadbolt, N. Matsuda, M. Oguma, M. Itoh, G. D. Marshall, M. G. Thompson, J. C. F. Matthews, T. Hashimoto, J. L. O. Brien, and A. Laing, "Universal linear optics," Science **349**, 711–716 (2015).

[26] A. S. Clark, L. G. Helt, M. J. Collins, C. Xiong, K. Srinivasan, B. J. Eggleton, and M. J. Steel, "Nonlinear Optics for Photonic Quantum Networks," in "All-Optical Signal Processing," , S. Wabnitz and B. J. Eggleton, eds. (Springer, Switzerland, 2015), chap. 12, pp. 355–412, 1st ed.

[27] L. G. Helt, J. E. Sipe, and M. J. Steel, "Spontaneous parametric downconversion in waveguides: What's loss got to do with it?" New J. Phys. **17**, 013055:1–17 (2014).

[28] E. Brainis, "Four-photon scattering in birefringent fibers," Phys. Rev. A **79**, 023840:1–14 (2009).

[29] Q. Lin, F. Yaman, and G. P. Agrawal, "Photon-pair generation in optical fibers through four-wave mixing: Role of Raman scattering and pump polarization," Phys. Rev. A **75**, 023803:1–20 (2007).

[30] M. J. Collins, A. S. Clark, J. He, D.-Y. Choi, R. J. Williams, A. C. Judge, S. J. Madden, M. J. Withford, M. J. Steel, B. Luther-Davies, C. Xiong, and B. J. Eggleton, "Low Raman-noise correlated photon-pair generation in a dispersion-engineered chalcogenide As_2S_3 planar waveguide," Opt. Lett. **37**, 3393:1–3 (2012).

[31] M. J. Collins, C. Xiong, I. H. Rey, T. D. Vo, J. He, S. Shahnia, C. Reardon, T. F. Krauss, M. J. Steel, a. S. Clark, and B. J. Eggleton, "Integrated spatial multiplexing of heralded single-photon sources," Nature Comm. **4**, 2582:1–7 (2013).

[32] A. Christ and C. Silberhorn, "Limits on the deterministic creation of pure single-photon states using parametric down-conversion," Phys. Rev. A **85**, 023829:1–6 (2012).

[33] Z. Yan, Y. Duan, L. G. Helt, M. Ams, M. J. Withford, and M. J. Steel, "Generation of heralded single photons beyond 1100 nm by spontaneous four-wave mixing in a side-stressed femtosecond laser-written waveguide," Appl. Phys. Lett. **107**, 231106:1–5 (2015).

[34] A. Pathak, *Elements of Quantum Computation and Quantum Communication* (CRC Press, 2013), 1st ed.

[35] J. Zhang, Y. Sun, and Q. Song, "Optimization of one-third harmonic generation in the presence of nonlinear phase modulations and power attenuation," Opt. Express **23**, 17407:1–14 (2015).

[36] A. Dot, A. Borne, B. Boulanger, K. Bencheikh, and J. a. Levenson, "Quantum theory analysis of triple photons generated by a $\chi^{(3)}$ process," Phys. Rev. A **85**, 023809:1–12 (2012).

[37] K. Bencheikh, F. Gravier, J. Douady, A. Levenson, and B. Boulanger, "Triple photons: a challenge in nonlinear and quantum optics," Comptes Rendus Physique **8**, 206–220 (2007).

[38] G. P. Agrawal, *Nonlinear Fiber Optics* (Elsevier, 2006), 4th ed.

[39] P. D. Drummond and Z. Ficek, *Quantum Squeezing* (Springer, 2014).

[40] Z. Yang, M. Liscidini, and J. Sipe, "Spontaneous parametric down-conversion in waveguides: A backward Heisenberg picture approach," Phys. Rev. A **77**, 033808:1–13 (2008).

[41] N. Quesada and J. E. Sipe, "Effects of time ordering in quantum nonlinear optics," Phys. Rev. A **90**, 063840:13 (2014).

[42] N. Quesada and J. E. Sipe, "Time-Ordering Effects in the Generation of Entangled Photons Using Nonlinear Optical Processes," Phys. Rev. Lett. **114**, 093903:1–5 (2015).

[43] A. Canagasabey, C. Corbari, Z. Zhang, P. G. Kazansky, and M. Ibsen, "Broadly tunable second-harmonic generation in periodically poled silica fibers." Opt. Lett. **32**, 1863–1865 (2007).

[44] N. Myrén, M. Fokine, O. Tarasenko, L.-E. Nilsson, H. Olsson, and W. Margulis, "In-fiber electrode lithography," J. Opt. Soc. Am. B **21**, 2085–2088 (2004).

[45] L. G. Helt, M. J. Steel, and J. E. Sipe, "Parasitic nonlinearities in photon pair generation via integrated spontaneous four-wave mixing: Critical problem or distraction?" Appl. Phys. Lett. **102**, 201106:1–5 (2013).

[46] J. E. Sipe, "Photons in dispersive dielectrics," Journal of Optics A **11**, 114006:1–7 (2009).

[47] W. Grice and I. Walmsley, "Spectral information and distinguishability in type-II down-conversion with a broadband pump," Phys. Rev. A **56**, 1627–1634 (1997).

[48] F. Gravier and B. Boulanger, "Triple-photon generation: comparison between theory and experiment," J. Opt. Soc. Am. B **25**, 98–102 (2008).

[49] J. E. Sharping, K. F. Lee, M. a. Foster, A. C. Turner, B. S. Schmidt, M. Lipson, A. L. Gaeta, and P. Kumar, "Generation of correlated photons in nanoscale silicon waveguides," Opt. Express **14**, 12388–12393 (2006).

[50] V. Grubsky and A. Savchenko, "Glass micro-fibers for efficient third harmonic generation," Opt. Express **13**, 6798–6806 (2005).

[51] L. G. Helt, "Nonlinear quantum optics in artificially structured media," Phd, University of Toronto (2013).

[52] L. G. Helt, Z. Yang, M. Liscidini, and J. E. Sipe, "Spontaneous four-wave mixing in microring resonators." Opt. Lett. **35**, 3006–3008 (2010).

[53] E. Y. Zhu, C. Corbari, A. Gladyshev, P. G. Kazansky, H. K. Lo, and L. Qian, "Multi-party Agile Quantum Key Distribution Network with a Broadband Fiber-based Entangled Source," Arxiv **175**, 661–663 (2015).

[54] W. P. Grice, R. S. Bennink, D. Earl, P. Evans, T. Humble, R. Pooser, J. Schaake, and B. Williams, "Multi-client quantum key distribution using wavelength division multiplexing," in "Proc. SPIE 8163, Quantum Communications and Quantum Imaging IX," , vol. 8163 (2011), vol. 8163, pp. 81630B–81630B–7.

[55] W. Grice, R. Bennink, P. Evans, T. Humble, R. Pooser, J. Schaake, and B. Williams, "Time-bin entanglement distribution on a wavelength-division-multiplexed network," in "CLEO: 2011 - Laser Science to Photonic Applications," (2011), pp. 1–2.

[56] B. Bell, A. Mcmillan, W. Mccutcheon, and J. Rarity, "On the effects of self- and cross-phase modulation on photon purity for four-wave mixing photon-pair sources," pp. 1–11 (2015).

[57] A. N. Whitehead and B. Russell, *Principia Mathematica* (Cambridge University Press, 1927), 2nd ed.

[58] W. H. Louisell, *Quantum Statistical Properties of Radiation* (Wiley, 1990).